RSC Advances

REVIEW

View Article Online
View Journal | View Issue

Cite this: *RSC Adv.*, 2021, **11**, 24254

Preparation and application of layered double hydroxide nanosheets

Yaping Zhang, * Huifang Xu and Song Lu

Received 27th April 2021
Accepted 21st June 2021

DOI: 10.1039/d1ra03289e

rsc.li/rsc-advances

Layered double hydroxides (LDH) with unique structure and excellent properties have been widely studied in recent years. LDH have found widespread applications in catalysts, polymer/LDH nanocomposites, anion exchange materials, supercapacitors, and fire retardants. The exfoliated LDH ultrathin nanosheets with a thickness of a few atomic layers enable a series of new opportunities in both fundamental research and applications. In this review, we mainly summarize the LDH exfoliation methods developed in recent years, the recent developments for the direct synthesis of LDH single-layer nanosheets, and the applications of LDH nanosheets in catalyzing oxygen evolution reactions, crosslinkers, supercapacitors and delivery carriers.

1 Introduction

Layered double hydroxides (LDH), also known as hydrotalcite-like anionic clay, are a class of ionic lamellar compounds consisting of positively charged brucite-like layers and charge compensating anions and solvation molecules in the interlayer region. Generally, the formula of LDH can be described as $[M^{II}_{1-x}M^{III}_{x}(OH)_2]^{x+}(A^{n-})_{x/n}\cdot mH_2O$, where M^{II} represents bivalent metal cations, such as Mg^{2+}, Zn^{2+} or Ni^{2+}, and M^{III} represents trivalent metal, such as Al^{3+}, Ga^{3+}, Fe^{3+} or Mn^{3+}, and x is the mole ratio of $M^{III}/(M^{II} + M^{III})$, which is normally between 0.17 and 0.33,[1] and subject to change for various applications. LDH can also contain M^{+} and M^{4+} cations, such as Li^{+} and Ti^{4+}, but these are limited to specific examples. A^{n-} is the intercalated charge balancing anions.[2–4]

LDH have found widespread application in various fields, including photochemistry,[5–12] adsorption,[13,14] CO_2 capture,[15–20] drug delivery[21–23] and fire retardant additives,[24–29] however, the extent of their application as well as overall performance are extremely restricted by the fact that the unavoidable aggregation of the lamellar LDH flakes.

In the past decade, the synthesis of two-dimensional (2D) nanosheets of layered solids, such as metal chalcogenides,[30] metal phosphates and phosphonates,[31] layered metal oxides,[32–35] as well as layered double hydroxide,[36,37] have attracted tremendous attention. The 2D nanosheet, with a thickness of approximately one nanometer and a lateral size ranging from submicrometer to several tens of micrometers, possesses a higher specific surface area and more active sites, can be used for both fundamental studies and as a building block to fabricate a variety of functional materials.[38] Exfoliation of LDH is an important route to produce positively charged thin platelets with a thickness of a few atomic layers, which can be used in series of fields. A prevailing example is as highly efficient oxygen evolution electrocatalysts.[39–41] Today the synthesis of LDH nanosheets is of tremendous importance in both fundamental research and for the exponentially growing applications,[42,43] such as catalysis, polymer composites, electronic materials, magnetic materials, and nanostructured materials.[3] There are typically two categories of approaches to synthesize LDH nanosheets: top-down exfoliation and bottom-up direct synthesis methods. Exfoliation of layered materials is an interesting route for producing positively charged thin platelets, which typically constitutes a two-step process: the layered materials are first intercalated by macromolecule to increase the interlayer distance, and then the exfoliation step is developed to obtain exfoliated nanosheets. However, comparing with cationic clays such as lapinite® and montmorillonite which can be exfoliated into single layer sheets in aqueous suspension, LDH are more difficult to be exfoliated due to their high charge density and the high anion content. In addition, extensive interlamellar hydrogen bonding networks lead to a tight stacking of the lamellae. Therefore, new techniques need to be developed to successfully exfoliate LDH into nanosheets. While the bottom-up method is a relatively simple one-step process to directly prepare inorganic nanosheets from appropriate precursors.

LDH nanosheets synthesized by top-down exfoliation, such as in alcohols, toluene, polymers/monomers, CCl_4, formamide, have been detailed discussed in previous reviews.[3,44] In this review article, methods based on top-down exfoliation developed in recent years and methods to prepare LDH nanosheets based on bottom-up direct synthesis methods are discussed in detail, with a focus on the preparation mechanism. We also provide an overview of recent applications of LDH nanosheets,

Pharmacy College, Henan University of Chinese Medicine, Zhengzhou, 450008, PR China. E-mail: ypzhang0521@163.com

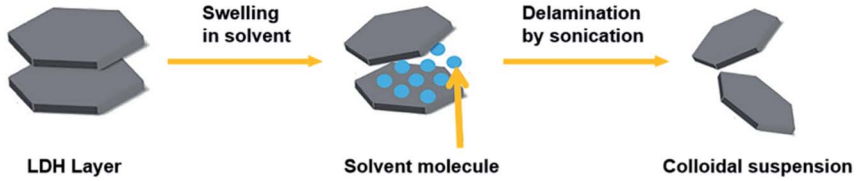

Fig. 1 A general process of exfoliating LDH.[46]

especially new applications in water splitting reactions, polymer nanocomposites, supercapacitors and drug delivery hosts.

2 Preparation of LDH nanosheets

The exfoliation of LDH has always been a hot topic. Comparing with other layered inorganic compounds, LDH are difficult to be exfoliated due to their high layer charge density.[45] In addition, the nanosheet dispersion obtained by exfoliation is unstable, and it is easy to self-assemble to restore the layered structure of LDH. Initially, LDH were exfoliated by inserting anionic organic guests (such as amino acids or surfactants) into the interlayer space and dispersing in a suitable solvent with the assistance of ultrasonication (Fig. 1).[46] After that, exfoliation in aqueous solution by electrostatic repulsion was developed.[47] Then, formamide was found as an ideal solvent, which made the direct exfoliation of LDH without being pre-intercalated by organic species in interlayer space was achieved. Presently, more and more efficient approaches to prepare LDH nanosheets were developed, such as laser ablation, the exfoliation process can be finished in several minutes. Traditional exfoliation approaches have been detailed discussed elsewhere,[36,44] therefore, we will discuss the exfoliation approaches developed in recent years and the future of this area.

2.1 Exfoliation or top down methods

2.1.1 Exfoliation in aqueous solution. Chen *et al.*[48] proposed a method to prepare 2D ultrathin nanosheets of Co–Al LDH by exfoliating in aqueous solution of L-asparagine. Co–Al–CO_3 LDH was pre-synthesized by a conventional coprecipitation method, after salt–acid treatment, the exfoliation of Co–Al LDH was performed: the mixture of LDH and L-asparagine saturated aqueous solution was mixed by ultrasonication, after vigorous oscillation, the unexfoliated particles was removed by centrifugation, and a translucent colloidal suspension of Co–Al LDH nanosheets was obtained. The TEM and SAED images indicated the exfoliated nanosheets were successfully obtained with intact micro-crystal structure (Fig. 2). The successful of the exfoliation was mainly due to that L-asparagine, which has a similar structure to formamide, is a water-soluble amino acid, its carbonyl groups had a strong interaction with LDH layers, and its amino groups made the interlayer interactions weakened, ultimately leaded to the exfoliation of the Co–Al LDH.

Zhang *et al.*[49] reported a new strategy to exfoliate inorganic LDH in aqueous solution by use of zwitterionic surfactants. The zwitterionic surfactants (sodium capryloamphoacetate (SC) and sodium lauroamphoacetate (SL)) were firstly intercalated into the decarbonated LDH by ion exchange, then a certain amount of surfactant-intercalated LDH was dispersed in acid solution with initial pH values of 2.0 and the mixture was stirred at room temperature for 2 days. The yield for the exfoliated MgAl-SC-LDH and MgAl-SL-LDH were 48% and 49% respectively. The AFM images (Fig. 3) indicated that, for the MgAl-SC-LDH, the average thickness was 0.721–1.433 nm, for the MgAl-SL-LDH the average thickness was 0.871–2.194 nm, which proved the surfactant intercalated LDH were successfully exfoliated into

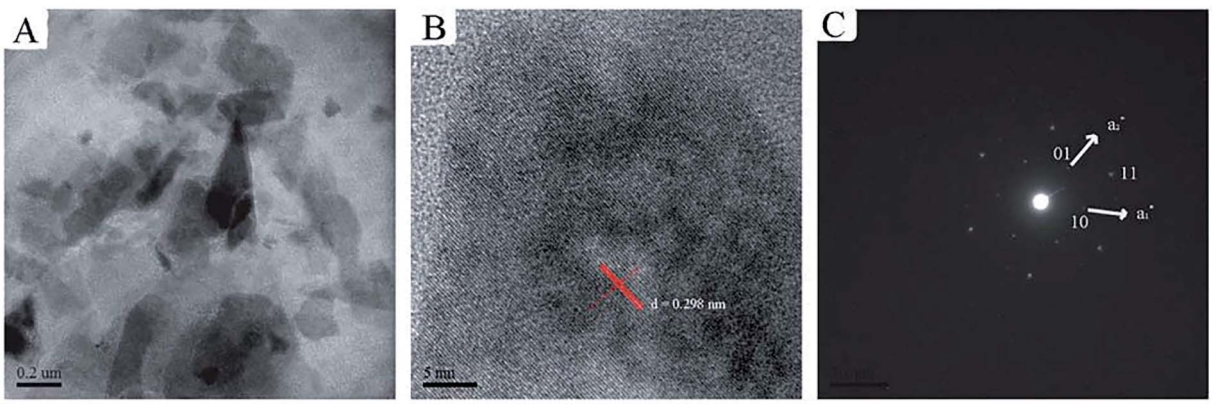

Fig. 2 (A) TEM image, (B) HRTEM image and (C) SAED pattern of the exfoliated Co–Al LDH nanosheets.[48] Reproduced with permission from ref. 48. Copyright 2013. The Royal Society of Chemistry.

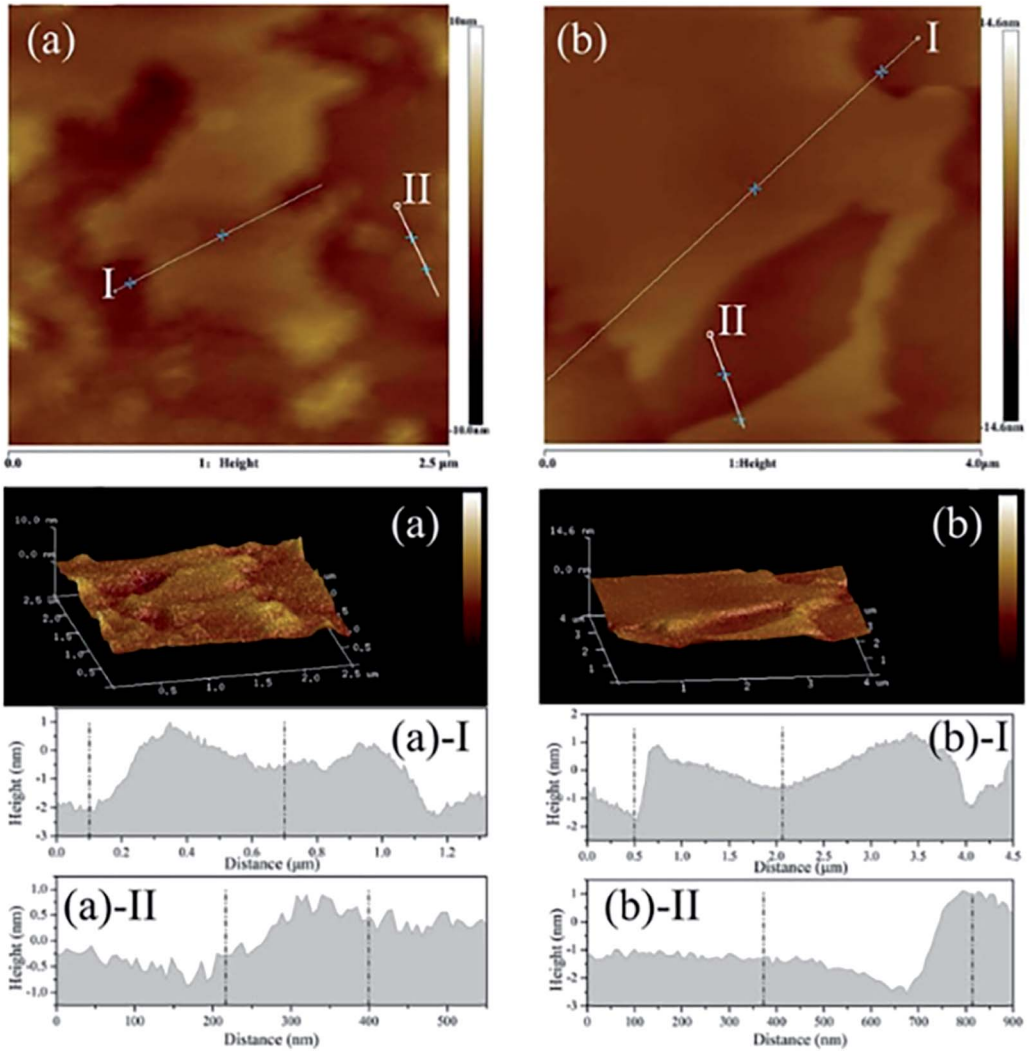

Fig. 3 The AFM image, 3D surface image and height profile of exfoliated LDH. (a) MgAl-SC-LDH; (b) MgAl-SL-LDH. Reproduced with permission from ref. 49. Copyright 2019. Taylor & Francis Group, LLC.

nanosheets. The authors believed that the electrostatic repulsion was the main factor that affects the exfoliation. The zwitterionic surfactants possess positively and negatively charged head groups simultaneously, there is an isoelectric point or isoelectric area within a certain pH or pH range, at the isoelectric point or isoelectric area the anionic and cationic groups can neutralize each other.[50] Above the isoelectric point, the zwitterionic exhibits an anionic character, SC or SL can be intercalated into LDH by ion exchange, when below the isoelectric point, the SC or SL converts to cationic species, resulting the exfoliation of LDH by electrostatic repulsion.

2.1.2 Exfoliation at low temperatures. Wei *et al.*[51] developed a novel and efficient method for the exfoliation of Zn/Al–Cl^-–LDH using NaOH/urea aqueous solution at low temperatures. This work was mainly taking advantage of that the alkali and urea aqueous solution can dissolve cellulose with strong inter- and intra-molecular hydrogen bonding at low temperatures,[52,53] the structure of LDH and cellulose has much in common, thus the author believed that the hydrogen bond and lamellar structure of LDH could also be destroyed using NaOH/urea aqueous solution at low temperatures. In their work, a series of NaOH/urea aqueous solution with 6–9 wt% NaOH and 10–15 wt% urea concentration were prepared at room temperature and precooled to −10 °C, then a certain amount of the pre-prepared Zn–Al LDH was added to the mixed solution and stirred vigorously for 3 min. After removing the not fully exfoliated LDH by centrifugation, the exfoliated Zn–Al LDH colloidal suspension was obtained. The thickness of the obtained LDH nanosheets was *ca.* 0.6 nm, which corresponding to the thickness of single-layer LDH. The further study of the mechanism demonstrated that the exfoliation of LDH in NaOH/urea aqueous solution was because of the formation of hydrates in alkali and urea solution at low temperature. As shown in Fig. 4, the NaOH hydrate intercalated into the LDH interlayer and attached onto the host layers, the original hydrogen bond network between the LDH layers was broken and form a new

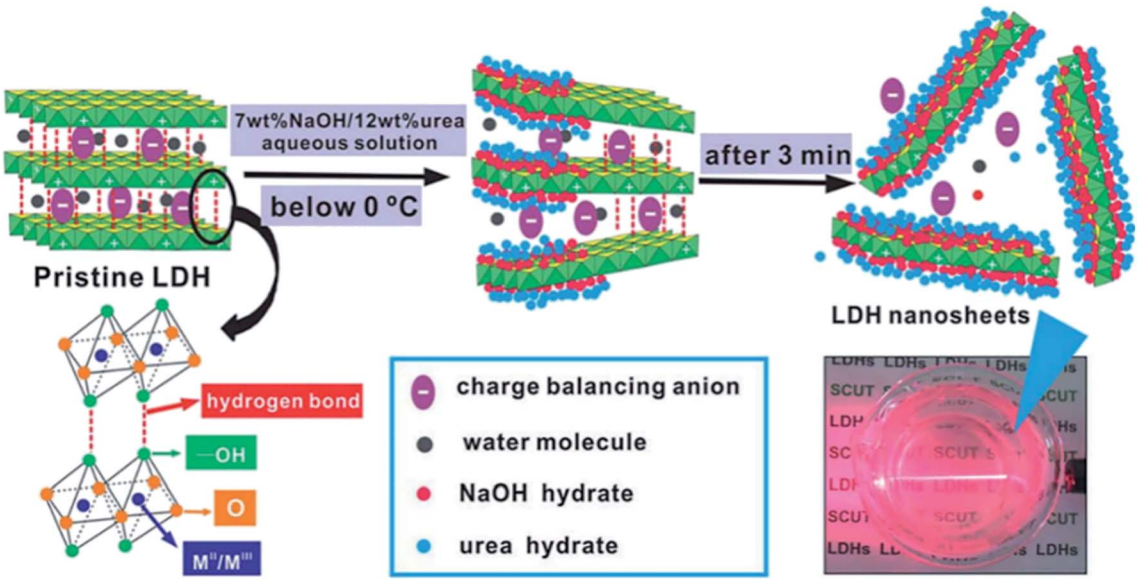

Fig. 4 The schematic diagram of delamination of LDH in precooled NaOH/urea aqueous solution.[51] Reproduced with permission from ref. 51. Copyright 2014 The Royal Society of Chemistry.

hydrogen bond network between the hydroxyl groups on the LDH layers and NaOH hydrate. Urea hydrates can easily self-assembled at the surface of the NaOH hydrogen-bonded host layers of LDH to stabilize the LDH nanosheets suspension and preventing the aggregation. The combination of the NaOH and urea solution destroyed the original hydrogen bond network between the LDH layers, leading the rapid exfoliation of LDH.

2.1.3 Dry exfoliation. Although the liquid exfoliation can obtain single layer nanosheets, it also has certain defects, such as time consuming, expensive, and requires toxic compounds. Furthermore, the solvent molecules used in the exfoliation often adsorbed on the surface of the as-exfoliated LDH nanosheets, and once the solvent molecules have been removed to obtain the powder products, the LDH nanosheets prone to restack into bulk LDH, which limited their further application.

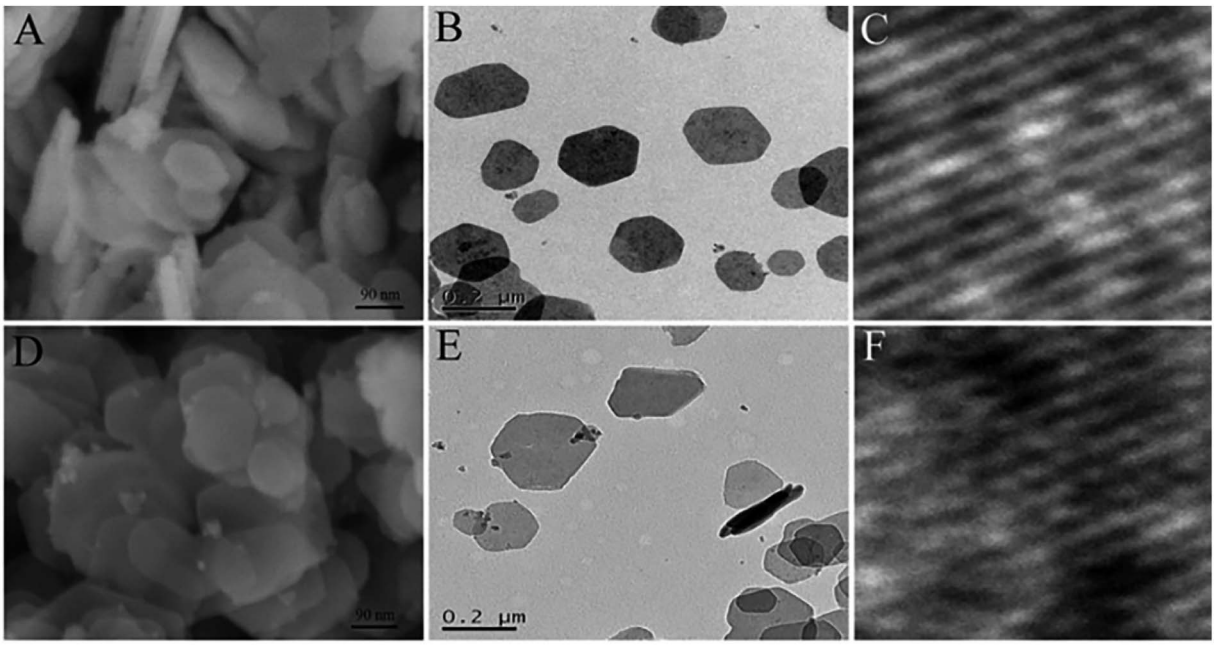

Fig. 5 SEM, TEM and HRTEM images of the bulk CoFe LDH (A–C) and the ultrathin CoFe LDH-Ar nanosheets (D–F). Reproduced with permission from ref. 54. Copyright 2017 John Wiley & Sons, Inc.

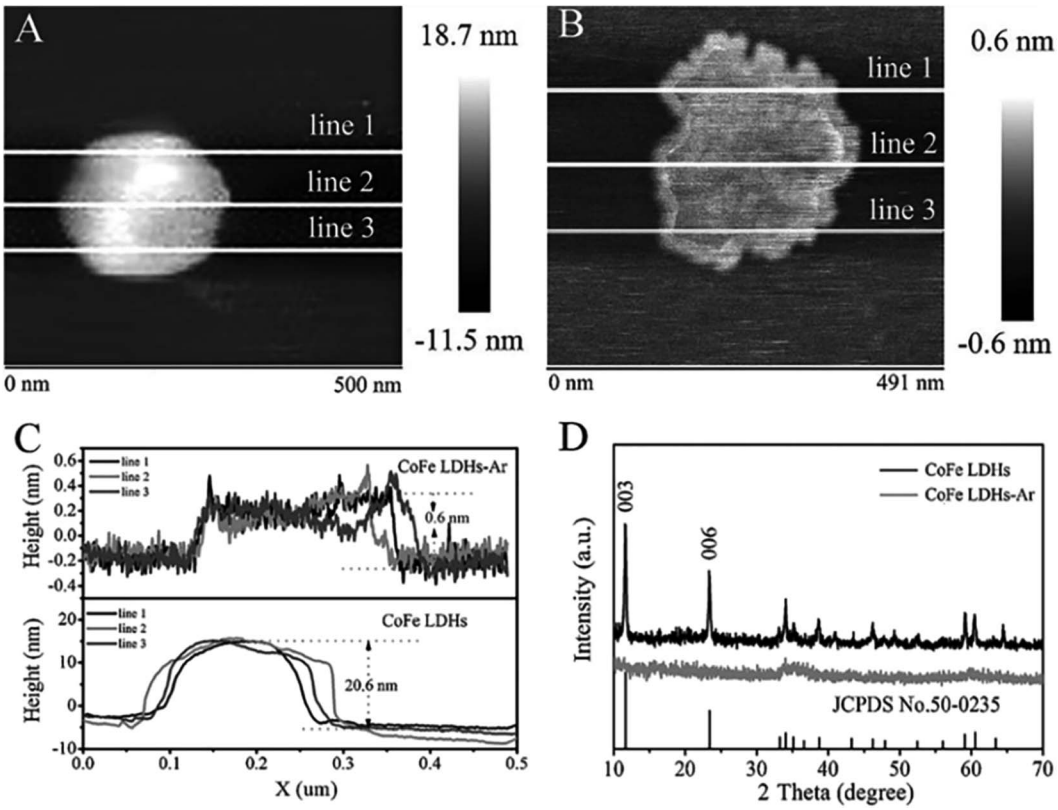

Fig. 6 AFM images of (A) bulk CoFe LDH and (B) ultrathin CoFe LDH-Ar nanosheets. (C) The corresponding height curves and (D) XRD patterns of the bulk CoFe LDH and ultrathin CoFe LDH-Ar nanosheets. Reproduced with permission from ref. 54. Copyright 2017 John Wiley & Sons, Inc.

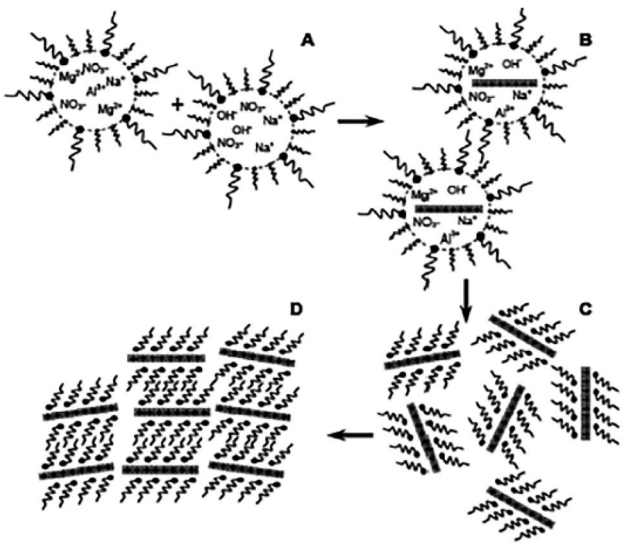

Fig. 7 Schematic representation of the nucleation and growth of LDH platelets. Reproduced with permission from ref. 55. Copyright 2006 The Royal Society of Chemistry.

In 2017, Wang *et al.*[54] developed a novel method called "dry exfoliation" to obtain ultrathin CoFe LDH nanosheets. The bulk CoFe LDH with a molar ratio of Co/Fe 2 : 1 were pre-synthesized by a hydrothermal method, then they were exfoliated into ultrathin LDH nanosheets by Ar plasma etching, which destroys the ionic bonds and hydrogen bonds in the interlayers of the bulk LDH, disturbing the normal charge balance and separating the positively charged brucite-like host layers from each other.

SEM, TEM and AFM results (Fig. 5 and 6) indicated that the pristine CoFe LDH had multilayer structure with a lateral size of 50–300 nm and a thickness of 20.6 nm. The X-ray diffraction (XRD) patterns shown that all of the diffraction peaks of the bulk CoFe LDH could be well indexed to JCPDS No. 50-0235 (Fig. 6D), which demonstrated that the bulk CoFe LDH have been synthesized successfully. The interlayer distance of the bulk CoFe LDH is 7.6 Å, this confirmed that carbonate ions were present between the layers. After treating with Ar plasma etching for 60 min, the ultrathin CoFe LDH nanosheets, marked as CoFe LDH-Ar, were produced. SEM, TEM and AFM results showed that the CoFe LDH-Ar preserved the nanosheet structure with a thickness of 0.6 nm (corresponding to the thickness of a monolayer), which demonstrated that the bulk CoFe LDH have been successfully exfoliated by the Ar plasma etching, which should destroy the ionic bonds in the interlayers of the bulk CoFe LDH. The XRD characterization (Fig. 6D) showed that the diffraction peaks corresponding to the (003) and (006) planes of CoFe LDH-Ar disappeared, which also indicated the

successful exfoliation of bulk CoFe LDH into ultrathin CoFe LDH nanosheets.

Compared with liquid exfoliation, dry exfoliation has many advantages, such as clean, time-saving, non-toxic, and could avoid the adsorption of solvent molecules, it provided a new way to exfoliate 2D materials and provided more opportunities for the discovery of novel applications for LDH-based materials.

2.2 Direct synthesis methods

Bottom-up direct synthesis method is an excellent route to synthesis of LDH nanosheets, its process is relatively simple and there is no need to pre-synthesis of layered LDH. At present, the methods for directly synthesizing LDH nanosheets are mainly chemical approaches, such as creating "microreactors" utilizing the microemulsion method and mechanical methods, inhibiting the growth of layers by a layer growth inhibitor, washing the solid obtained from traditional coprecipitation method with aqueous miscible organic solvent, synthesizing directly in organic solvents, and mechanical methods, such as applying a laser beam on metals in aqueous solution, establishing a quick mixing environment using a special reactor, grinding nitrate in a suitable solvent.

2.2.1 Chemical methods. Hu *et al.*[55] reported a facile one-step synthesis of LDH monolayers in a reverse microemulsion in 2005. In their work, the traditional aqueous co-precipitation system (magnesium salt and aluminum salt at pH $\geq$ 10) was adopted into an oil phase of isooctane with sodium dodecyl sulfate (SDS) as surfactant and 1-butanol as co-surfactant to prepare LDH monolayers. The synthesis process is shown in Fig. 7. The pre-prepared aqueous phase was dispersed into the oil phase to obtain droplets surrounded by dodecyl sulfate groups (DDS). And these droplets acted as nano-reactors to provide limited space and nutrients for the growth of LDH platelets, as a result, the size of the LDH platelets was controlled both in diameter and thickness.

AFM was applied to characterize the obtain LDH nanosheets.[55] The typical topology of isolated oval objects is presented in Fig. 8a, we can see that all the particles have a uniform diameter distribution centered around 40 nm. Fig. 8b shows that all these particles have a height of *ca.* 1.5 nm. The thickness of Mg_2Al-LDH single layer is 0.47 nm,[56–58] thus, the particles shown in Fig. 8 are corresponding to three mono-layers without considering the interlayer spacing expanded by the charge-balancing DDS anions. However, the elemental analysis result indicated the presence of the DDS anions on the LDH platelets, combining the basal spacing of DDS intercalated LDH, it can be concluded that the LDH layers formed in the reverse micro-emulsion have a mono-layer structure.

In the above synthesis method, anionic surfactants are often difficult to elute as counter anions adsorbed on the surface of LDH nanosheets, thus, in order to avoid the complex purification process, Bellezza *et al.*[59] developed a cationic surfactant based reverse micro-emulsion method to prepare LDH nanosheets, avoiding the removal of surfactant.

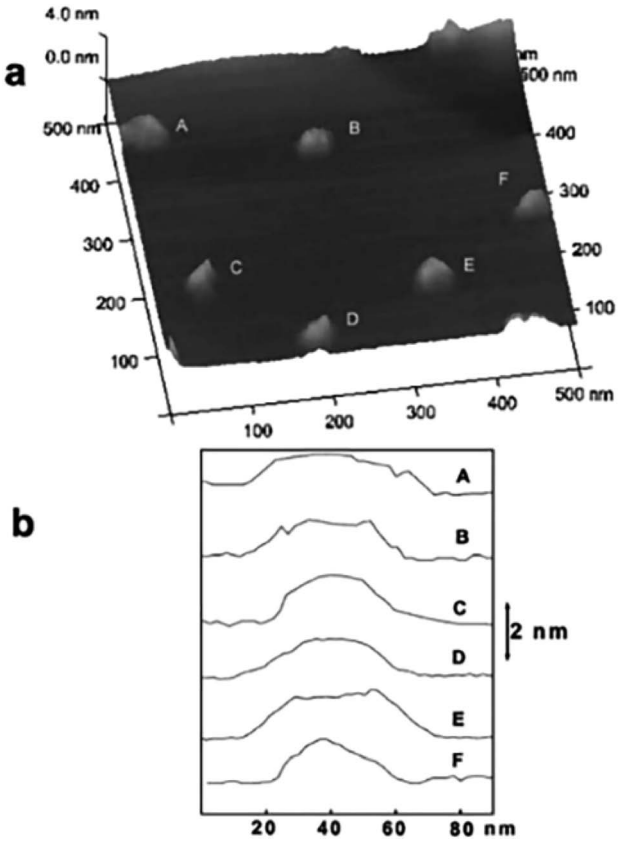

Fig. 8 (a) AFM image of the particles synthesized by a reverse micro-emulsion method deposited on a highly oriented pyrolytic graphite (HOPG) surface; (b) cross-sectional analysis of the labeled particles in (a) showing the dimensional profiles. Reproduced with permission from ref. 55. Copyright 2006 The Royal Society of Chemistry.

In 2001, Yan *et al.*[60] developed a novel single-step method to prepare large scale LDH nanosheets. $Mg(NO_3)_2 \cdot 6H_2O$, $Al(NO_3)_3 \cdot 9H_2O$, and urea were dissolved in 100 mL 30% H_2O_2, then the mixture solution was transferred into a Teflon tube Teflon-lined autoclave and heated at 150 °C for 24 h. The suggested scheme of the synthetic process was illustrated in Fig. 9A, part of H_2O_2 decomposed into H_2O and O_2 when heated, with the rising of temperature the LDH gradually formed, authors believed that during the synthetic process, part of the H_2O_2 and O_2 could be positioned in the interlayer of LDH. The rapid decomposition of H_2O_2 occurred after formulation of LDH, and the violent movement of O_2 in the interlayers resulted the increase of the spacing between layers and the diminished of the electrostatic interaction between the layers, leading to the separation of LDH layers. Fig. 9B is the AFM image of the prepared nanosheets, the result showed that the average thickness of the nanosheets was about 1.44 nm, corresponding to the theoretical thickness of approximately two LDH layers ($0.76 \times 2 = 1.52$ nm).

Wang *et al.*[61] reported a facile method called aqueous miscible organic solvent treatment (AMOST) for the synthesis of

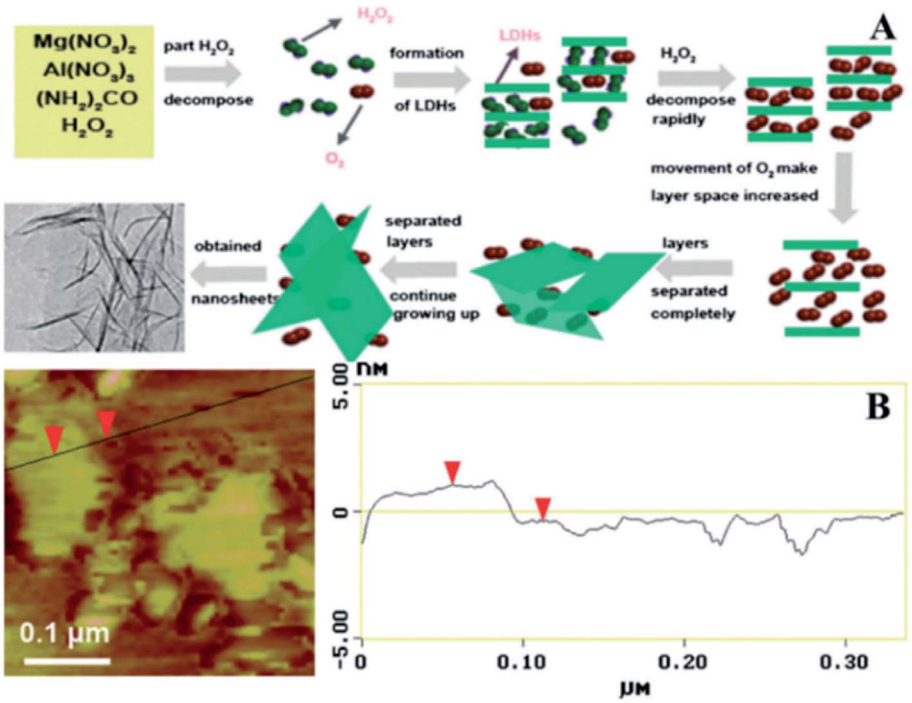

Fig. 9 (A) Proposed scheme for the preparation of exfoliated Mg_2/Al–LDH nanosheets; (B) AFM image of the synthesized ultrathin sheets. Reproduced with permission from ref. 60. Copyright 2012 Elsevier Inc.

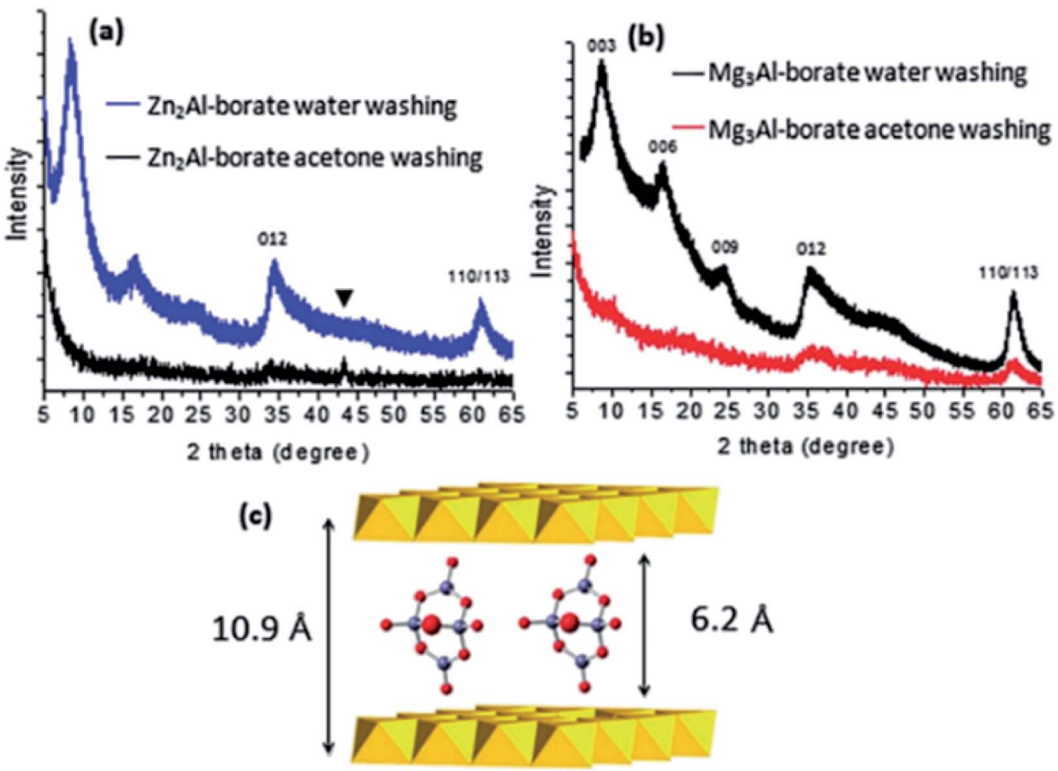

Fig. 10 (a) Comparison of the XRD patterns of Zn_2Al-borate LDH synthesized by conventional co-precipitation (washing with water) and the AMOST method; (b) Mg_3Al-borate LDH synthesized by conventional co-precipitation (washing with water) and the AMOST method; (c) schematic illustration of the structure of $[B_4O_5(OH)_4]^{2-}$ with the LDH layers. Reflections from the sample holder. Reproduced with permission from ref. 61. The Royal Society of Chemistry.

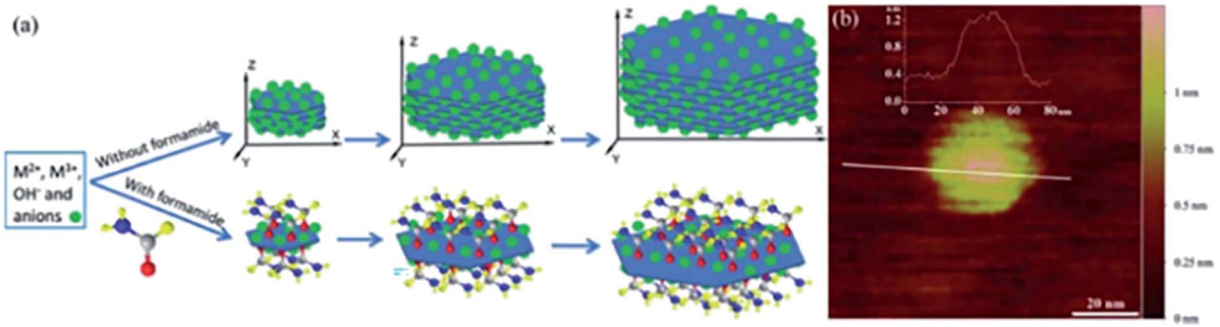

Fig. 11 (a) Direct growth of LDH single-layer nanosheets with the assistance of layer growth inhibitors (not drawn to scale); (b) AFM image of a pseudohexagonal Mg_4/Al–LDH nanosheet.[62] Reproduced with permission from ref. 62. Copyright 2015 The Royal Society of Chemistry.

LDH nanosheets. And what's interesting is that it is the first report of LDH powders that still remain exfoliated in the dry phase. $Zn(NO_3)_2 \cdot 6H_2O$ and $Al(NO_3)_3 \cdot 9H_2O$ solution were added dropwise to H_3BO_3 solution. The pH of the precipitation system was controlled at *ca.* 8.3 with NaOH solution. The mixture system was purged with N_2 gas, followed by aging at 65 °C overnight. The obtained solid were washed with water until pH was close to 7. After that, the slurry washed by water was re-dispersed in acetone and stirred for 1 h at room temperature, then it was filtered and washed thoroughly with acetone again. At last the product was dried at 65 °C overnight. The structural changes of the samples were characterized by XRD (Fig. 10). The $00l$ (l = 3, 6, 9…) Bragg reflections of the conventional water washed samples could be observed obviously, while for the samples obtained by AMOST method, the $00l$ Bragg reflections disappeared but low intensity 012 and 110/113 Bragg reflections were observed, which indicated that the LDH were completely exfoliated.

The authors believed that the solvent used in the final dispersion was the key to control the hydrophobicity of the LDH platelets, and it must be 100% miscible with water. In the process of nucleation and growth of the LDH in water, the

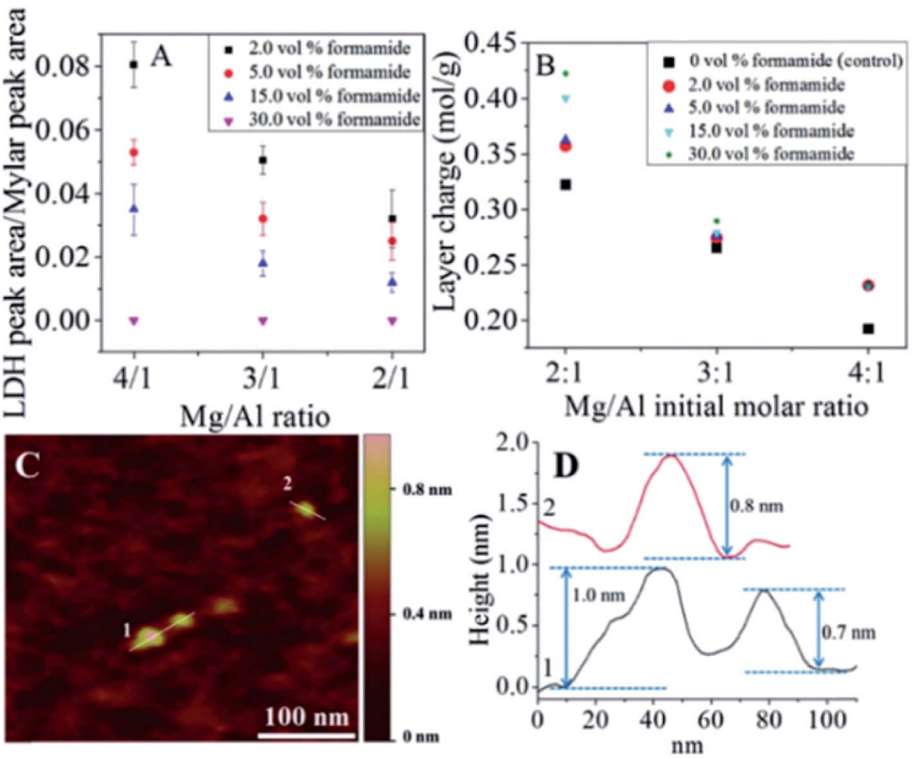

Fig. 12 (A) LDH characteristic peak to internal reference peak area ratios. (B) MgAl–LDH layer charge at different Mg/Al formulation molar ratios and formamide concentrations. (C) Representative AFM image of Mg_2Al–LDH prepared in 30.0 vol% formamide and the corresponding height profile (D). Reproduced with permission from ref. 63. Copyright 2016 The American Chemistry Society.

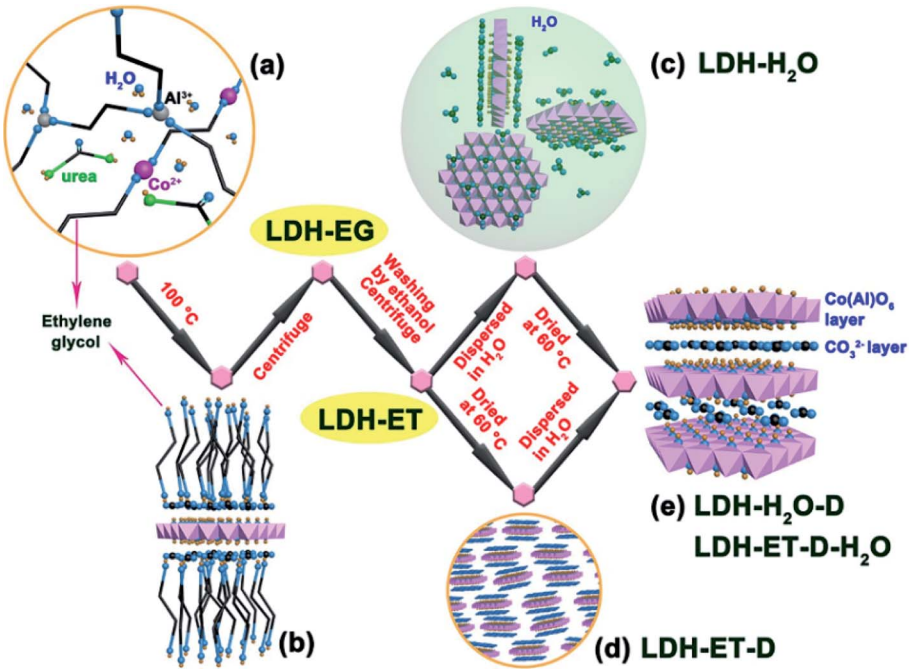

Fig. 13 Schematic illustration for formation and structure of CoAl–CO_3^{2-} SL-LDH and CoAl–CO_3^{2-} LDH: (a) ethylene glycol (EG) solution of reactants; (b) adsorption of EG molecules on the surface of a SL-LDH nanosheet in reaction; (c) completely dispersed SL-LDH in water; (d) disorderly stack of SL-LDH in the dried state; and (e) LDH assembly structure from generated SL-LDH. Reproduced with permission from ref. 64. Copyright 2017 The American Chemistry Society.

primary brucite-like metal hydroxide nanosheets were surrounded by charge compensating counter anions, and this arrangement was highly solvated by water molecules because of its high surface charge density. During the aging and washing steps, the LDH nanosheets combined with each other and stacked layer-by-layer. The water acted to both solvate the anions and also bond the individual metal hydroxide nanosheets together through extensive hydrogen bonding. When water molecules were replaced by acetone molecules, the LDH could be exfoliated and dispersed easily. Due to the low boiling point of acetone, the facile loss of interlayer acetone molecules lead to the ready collapse of an ordered stacked structure, and the formation of high surface porous materials with the specific surface areas and total pore volumes increased up to 458.6 m^2 g^{-1} and 2.15 cm^3 g^{-1}.

Yu *et al.*[62] reported a one-step direct synthesis method to synthesize LDH single-layer nanosheets by adding formamide (23 vol%) as an inhibitor. The traditional co-precipitation route

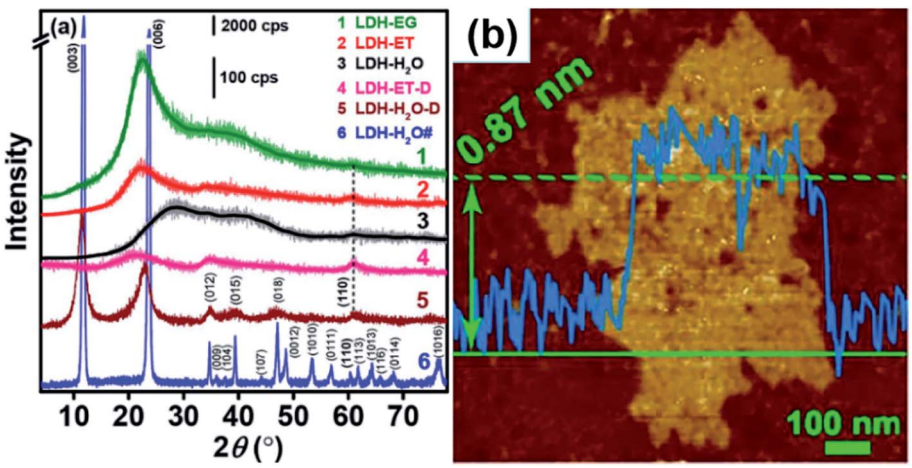

Fig. 14 (a) XRD patterns of different samples and (b) AFM image of LDH-H_2O. Reproduced with permission from ref. 64. Copyright 2017 The American Chemistry Society.

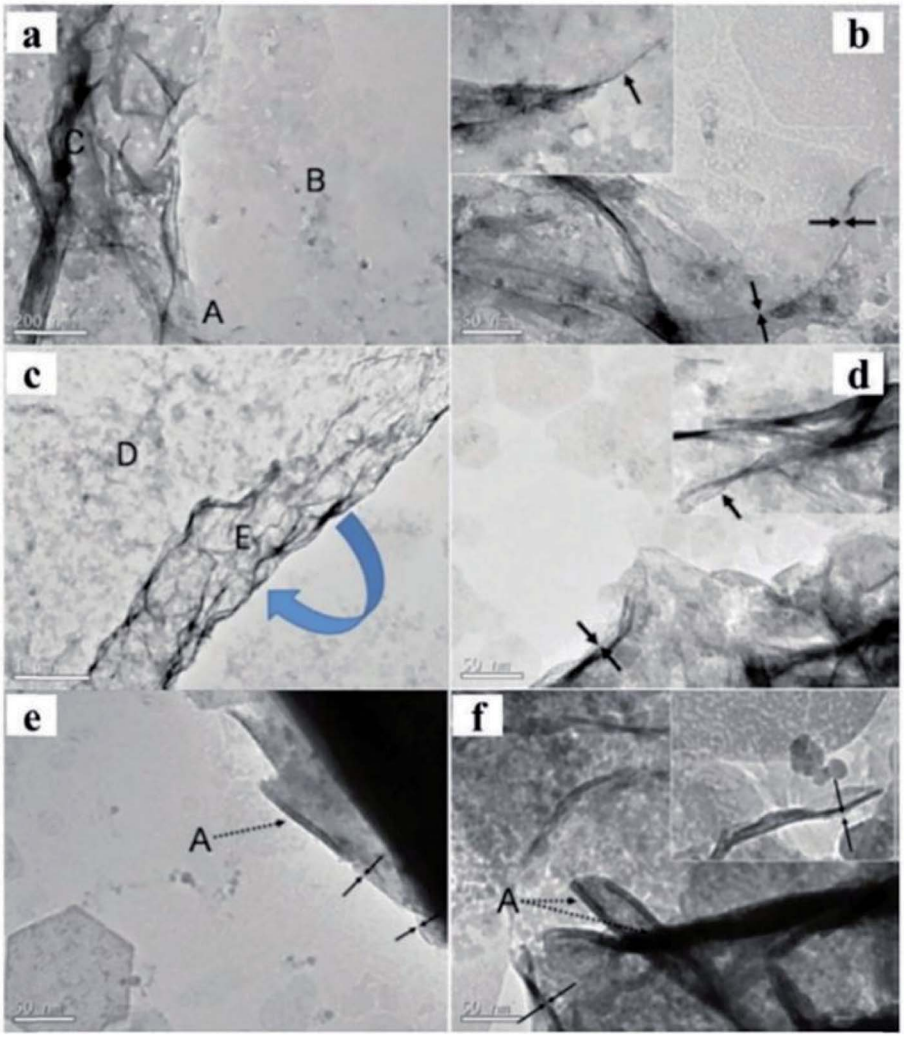

Fig. 15 TEM images of $Mg_{1.97}$/Fe and $Co_{0.96}$/Fe–LDH materials. Scale bars in the $Mg_{1.97}$/Fe–LDH images, (a and b), represent 200 nm and 50 nm, respectively. Scale bars in the $Co_{0.96}$/Fe–LDH images, (c and d), represent 1 mm and 50 nm, respectively. (e) $Co_{1.07}$/Al and (f) $Zn_{1.48}$/Al–LDH nanosheets. The dotted arrows marked by symbol "A" indicate the edges of the nanosheets seriously rolled because of the instability of the edges of the free-standing ultrathin LDH layers. Both scale bars represent 50 nm in (e and f). Insets in images (b, d, and f) display the corresponding side views. Reproduced with permission from ref. 68. Copyright 2010 American Institute of Physics.

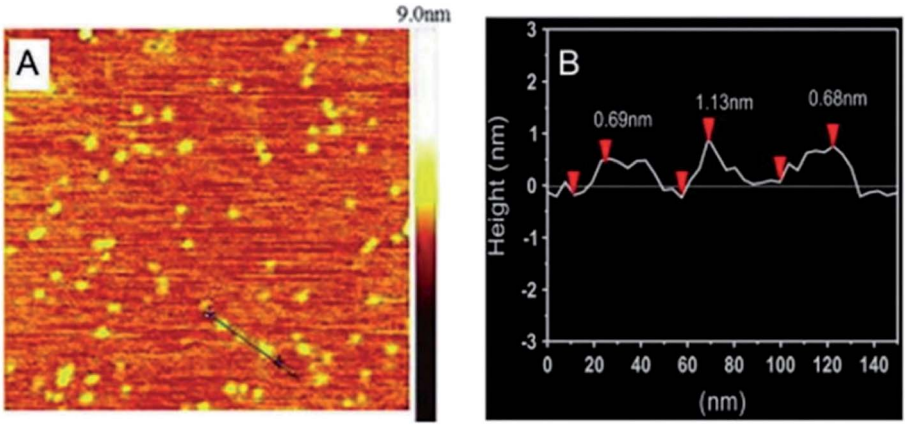

Fig. 16 (A) AFM image and height scale of the LDH nanosheets, and (B) sectional analysis along the black line marked in (A).[69] Reproduced with permission from ref. 69. Copyright 2014 Elsevier Inc.

was adopted with slight modified: a mixture solution (10 mL) composed of 0.040 M $Mg(NO_3)_2$ and 0.010 M $Al(NO_3)_3$ was added dropwise to the solution of $NaNO_3$ (10.0 mL, 0.010 M) containing 23 vol% formamide, and NaOH (0.25 M) solution was added under magnetic stirring at 80 °C to adjust pH of the above-mentioned system at *ca.* 10. After 10 minutes, the obtained sample was centrifuged and washed three times with water, single layer LDH nanosheets were obtained by re-dispersing the slurry in water. During the synthesis process, formamide molecules were adhered to the LDH nanosheet surface, due to its preferred interaction with the LDH layer surface and high dielectric constant (which resulted the interactions between layers weakened), LDH single-layer nanosheets were prepared (Fig. 11a).

The AFM image (Fig. 11b) demonstrated that the height of the prepared LDH single-layer nanosheets was *ca.* 0.8 nm, corresponding to the thickness of single-layer nanosheet with surface adsorbed anions and formamide molecules.

The authors further studied the effect of the concentration of formamide on the synthesis of LDH single layer nanosheets.[63] The result demonstrated that LDH single layer could be better prepared with the increasing volume percentage of formamide in the reaction system. And LDH with higher layer charge was beneficial to the formation of LDH single-layer nanosheets (Fig. 12A and B). As shown in Fig. 12C and D, the single layer features of the LDH prepared in 30 vol% formamide could be observed clearly.

The synthesis of single layer LDH with NO_3^- counterions has been extensively studied, however, the single layer LDH with CO_3^{2-} counterions was rarely reported. In 2017, Li *et al.*[64] first reported the simple direct synthesis of the CoAl–CO_3^{2-} LDH single layer nanosheets in ethylene glycol. The synthesis process was shown in Fig. 13, a certain amount of $Co(NO_3)_2 \cdot 6H_2O$, $Al(NO_3)_3 \cdot 9H_2O$ and urea were dissolved in 80 mL of ethylene glycol, and the obtained mixture solution was transferred into 100 mL Teflon-lined autoclave, following heated at 100 °C for 24 h. When preparing LDH with different Co/Al ratios, the total concentrations of metal ions and the urea concentrations were kept constant. The obtained suspension was naturally cooled to room temperature, and then centrifuged to get the sample, marked as LDH-EG. After that, the obtained LDH-EG was washed with ethanol (ET) and centrifuged for four times to get another sample, named as LDH-ET. The prepared LDH-ET sample was dried at 60 °C for 24 h and the solid sample, marked LDH-ET-D was obtained. Besides, the LDH-ET was dispersed into water by ultrasonication for 10 min and the aqueous colloids, marked as LDH-H_2O, was gained, the solid content of the aqueous colloids was ~3.87%. The solid sample, LDH-H_2O-D, was obtained by drying the LDH-H_2O colloid at 60 °C for 24 h. Additionally, the sample, marked as LDH-ET-D-H_2O, was obtained by dispersing the LDH-ET-D in water and the sample, marked as LDH-ET-D-H_2O-D, was obtained by drying the LDH-ET-D-H_2O at 60 °C for 24 h.

The XRD results (Fig. 14a) showed that, compared with LDH-H_2O# (synthesized in water), the XRD patterns of LDH-EG, LDH-ET, LDH-H_2O (gel, obtained by condensing the dilute colloid at 60 °C) and LDH-ET-D showed (110) and (012) but not (003) peaks, which indicated the presence of the single layer LDH. The AFM result (Fig. 14b) demonstrated that the single layer LDH nanosheets in LDH-H_2O have a height of ~0.85 ± 0.02 nm, corresponding to one $Co(Al)O_6$ layer sandwiched between two CO_3^{2-} layers. Authors believed that the successful preparation of CoAl–CO_3^{2-} single layer LDH probably arises from three reasons: (1) EG has strong chelation to metal ions,[65] which slowed the nucleation and growth of LDH crystals; (2) the growth along the [003] direction or assembly of the single layer

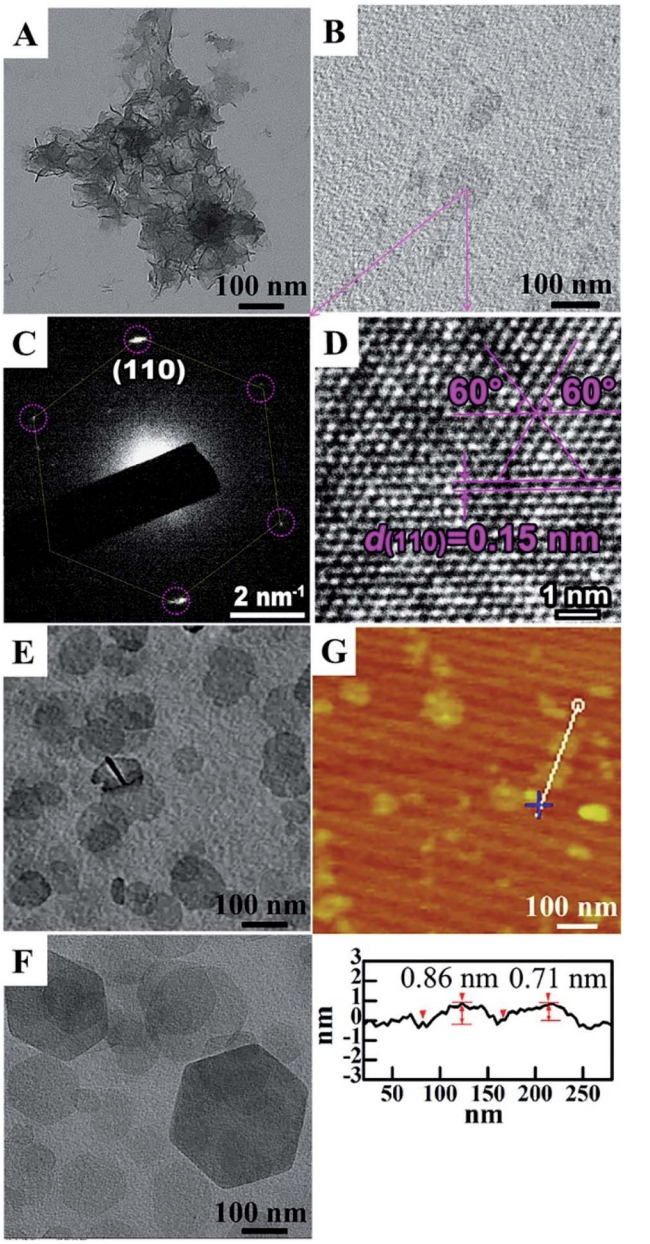

Fig. 17 TEM images of dispersions of (A) LDH single layer nanosheets gel, (B) LDH single layer nanosheets, (E) LDH single layer nanosheets after stacking at ~25 °C, and (F) peptized LDH platelets; (C) HR-TEM image and (D) SAED pattern of LDH single layer nanosheets; (G) AFM image and sectional analysis of the LDH single layer nanosheets.[70] Reproduced with permission from ref. 68. Copyright 2016 Elsevier Inc.

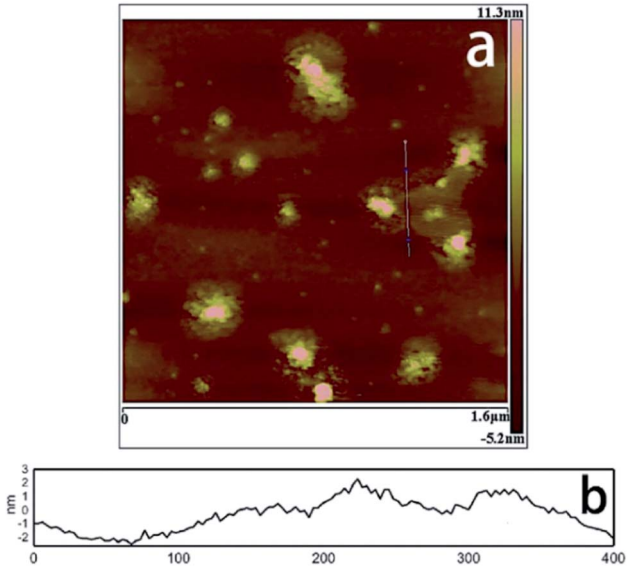

Fig. 18 AFM image (a) and height profile (b) of Co–Ni LDH monolayer nanosheets prepared at molar ratio of Co^{2+} to Ni^{2+} = 0.2. Reproduced with permission from ref. 71. Copyright 2016 Elsevier Inc.

LDH were prevented by the adsorption of EG molecules;[66,67] and (3) strong electrostatic repulsions between CO_3^{2-} layers and between $Co(Al)O_6$ layers with much structurally positive charge due to the low Co/Al ratio resulted that the single layer LDHs difficult to approach to each other. In summary, the direct synthesis of CO_3^{2-} LDH was reported for the first time and this work provided a simple method for the preparation of single layer LDH with CO_3^{2-}.

2.3 Mechanical methods

A new method to prepare LDH nanosheets in de-ionized water by a pulsed-laser ablation method was reported by Hur *et al.*[68] The Zn/Al, Co/Fe, Co/Al, and Mg/Fe–LDH colloidal nanosheets with a molecule thickness were obtained through this method. There are two consecutive steps in the laser ablation synthesis process: (1) laser ablation of trivalent metal target in de-ionized water at room temperature using a Q-switched Nd-yttrium aluminum garnet laser, and (2) the same laser ablation over a bivalent metal target in the pre-prepared trivalent metallic colloid. The power of the laser beam was 0.265 J cm^{-2} (1064 nm), the pulsed duration was 5.5 ns and the repetition rate was 10 Hz. The synthesis process took only 40 minutes. The TEM images (Fig. 15) showed that Mg/Fe and Co/Fe–LDH nanosheets displayed a rolling-and-folding morphology in the conjunction area, while the Co/Al and Zn/Al–LDH showed the edges intensively rolled. The thickness of the prepared LDH nanosheets were estimated by TEM, the Mg/Fe, Co/Fe, Co/Al, and Zn/Al–LDH nanosheets had a thickness of *ca.* 0.5, 0.48, 0.5, and 1.2 nm, respectively. Therefore, the laser ablation technique was deemed to have played a critical role in the formation of nanosheets.

Pang *et al.*[69] adopted the traditional coprecipitation method in a T-type micro-channel reactor in water for the synthesis of LDH nanosheets. A mixed salt solution (contained Mg^{2+} and Al^{3+} cations) with total concentration of 0.3 mol L^{-1} and $NH_3 \cdot H_2O$ solution (~7 wt%) were prepared in advance. And then the prepared two solutions were pumped into the micro-reactor (each at a flow rate of 20 mL min^{-1}) through two inlets. The AFM image (Fig. 16) indicated that the obtained LDH nanosheets have a diameter of 20–30 nm, and a thickness of *ca.* 0.68–1.13 nm, which corresponded to 1–2 brucite-like layers. This method is versatile for synthesizing various LDH nanosheets. The LDH nanosheets prepared by this method were in high quantities and could be used as building blocks for functional materials.

In 2016, our group developed a simple aqueous synthetic route to large-scale synthesis LDH single layer nanosheets.[70] This route includes three steps: aqueous coprecipitation, water-washing, and redispersion in water. In a typical procedure, $Mg(NO_3)_2/Al(NO_3)_3$ mixed salt solution (100 mL) with a total salt concentration of 0.3 mol L^{-1} and Mg/Al molar ratio of 2 and NH_3 H_2O solution (~7 wt%) were pre-prepared, then the two solution were added to a beaker simultaneously under stirring and N_2 protection, during this period, the pH of the reaction system was kept at ~10. After reaction for 10 min, the production was centrifuged and washed three times with water, and the LDH single layer nanosheets gel with a solid content (C_s) of ~8.5 wt% was obtained. Then the gel was redispersed in water by ultrasonication and the LDH single layer nanosheets dispersion (C_s = 2.0 g L^{-1}) was obtained. The TEM and AFM results showed that the LDH single layer nanosheets were successfully synthesized (Fig. 17).

Ma *et al.*[71] reported an ultra-large scale strategy under very moderate condition to synthesis Co–Ni LDH monolayer nanosheets. The detailed experiment process was as follows: a series

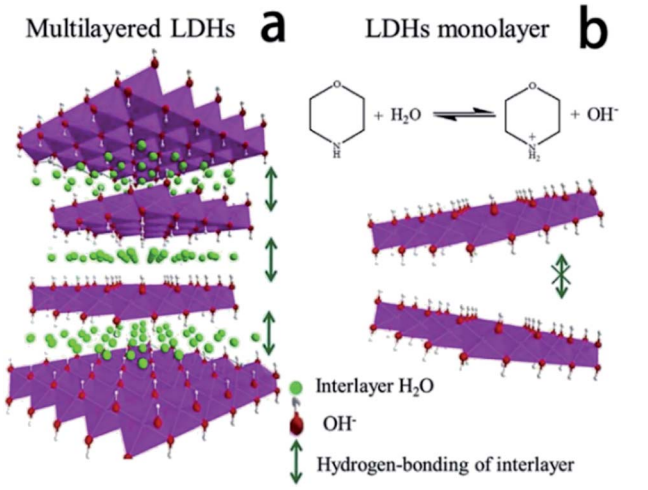

Fig. 19 Schematic illustration for the structure of multilayered Co–Ni LDH (a) and the formation mechanism of Co–Ni LDH monolayer nanosheets (b). Reproduced with permission from ref. 71. Copyright 2016 Elsevier Inc.

Table 1 A summary of LDH exfoliation/direct growth methods

No.	LDH	Interlayer anion	Dispersant	Process	Exfoliation	Ref.
1	CoAl-LDH	CO_3^{2-}	L-Asparagine saturated aqueous solution	The mixture of LDH and L-asparagine saturated aqueous solution was mixed by ultrasonication, after vigorous oscillation, the unexfoliated particles was removed by centrifugation	Partially exfoliated	48
2	MgAl-LDH	CO_3^{2-}	Aqueous solution of zwitterionic surfactants	Surfactant-intercalated LDH was dispersed in acid solution and stirred at room temperature for 2 days.	MgAl-SC-LDH: 48% MgAl-SL-LDH: 49%	49
3	Zn_7Al_3–LDH	Cl^-	NaOH/urea aqueous solution at low temperatures	Stirring a certain amount of Zn_7/Al_3–LDH in NaOH and urea solution system for 3 min	Successful[a]	51
4	Co_2Fe-LDH		Without solvent	Bulk CoFe LDH were treated with Ar plasma with power of 100 W	Not provided	54

Direct synthesis methods

No.	LDH	Interlayer anion	Reaction solvent system	Process	Exfoliation state	Ref.
1	Mg_2Al–LDH	DS^-	Isooctane with SDS and 1-butanol	LDH monolayers were synthesized in a reverse microemulsion system by a traditional aqueous co-precipitation method	Successful[a]	55
2	Mg_2Al–LDH	NO_3^-	30 wt% H_2O_2	$Mg(NO_3)_2 \cdot 6H_2O$, $Al(NO_3)_3 \cdot 9H_2O$, and urea were dissolved in 100 mL 30% H_2O_2, then the mixture solution was transferred into a Teflon tube Teflon-lined autoclave and heated at 150 °C for 24 h	Successful[a]	60
3	Zn_2Al-LDH Mg_3Al-LDH	BO_3^{3-}	Water	The LDH slurry washed by water was re-dispersed in acetone and stirred for 1 h at room temperature, then it was filtered and washed thoroughly with acetone again	Completely exfoliated	61
4	Mg_2Al–LDH Mg_4Al–LDH	NO_3^-	Water	A mixture solution composed of $Mg(NO_3)_2$ and $Al(NO_3)_3$ was added dropwise to the solution of $NaNO_3$ containing formamide	Successful[a]	62 and 63
5	$Co_{0.66}Al_{0.34}$-LDH $Co_{0.51}Al_{0.49}$-LDH	CO_3^{2-}	Ethylene glycol	A certain amount of $Co(NO_3)_2 \cdot 6H_2O$, $Al(NO_3)_3 \cdot 9H_2O$ and urea were dissolved in 80 mL of ethylene glycol, and the obtained mixture solution was transferred into 100 mL Teflon-lined autoclave, following heated at 100 °C for 24 h.	Successful[a]	64
6	$Zn_{1.48}Al$, $Co_{0.96}Fe$, $Co_{1.07}Al$, and $Mg_{1.97}Fe$–LDH	None	Water	Laser ablation of M(III) and M(II) metals in deionized water	Not provided	68
7	Mg_2/Al–LDH	NO_3^-	Water		Successful[a]	69

Table 1 (*Contd.*)

No.	LDH	Interlayer anion	Reaction solvent system	Process	Exfoliation state	Ref.
Direct synthesis methods						
8	Mg_2/Al–LDH	NO_3^-	Water	A mixed salt solution (containing Mg^{2+} and Al^{3+} cations) and an alkali solution containing NH_3 H_2O were pumped into the reactor through two inlets each at a flow rate of 20 mL min^{-1} A mixed salt solution (containing Mg^{2+} and Al^{3+} cations) and an alkali solution containing NH_3 H_2O were pumped into the reactor reaction for 10 min	Successful[a]	70
9	CoNi LDH	NO_3^-	None	$Ni(NO_3)_2.6H_2O$ and $Co(NO_3)_2.6H_2O$ mixture with different molar ratio of Co^{2+} and Ni^{2+} were prepared by grinding in a mortar, and then morpholine was added and the obtained mixture was ground for 6 min	Successful[a]	71

[a] Successful: the cited methods can produce single-layer nanosheets but containing multi-layered LDH as well.

of $Ni(NO_3)_2\cdot 6H_2O$ and $Co(NO_3)_2\cdot 6H_2O$ mixture with different molar ratio of Co^{2+} and Ni^{2+} were prepared by grinding in a mortar, and then morpholine was added (molar ratio of morpholine to metal ions was 4.1) and the obtained mixture was ground for 6 min, forming a sticky paste. After aging in a sealed beaker at room temperature for 10 h, the final product was washed with water and dried at 80 °C. AFM image (Fig. 18) indicated that the height of the nanosheets was inhomogeneous, the individual heights were about 1, 2 and 3 nm corresponding to one, two and three layers nanosheets respectively. For multilayered Co–Ni LDH (Fig. 19a), the multilayered structure was mainly balanced by the hydrogen bonding between the OH^- in layers and water molecules existing in interlayer region. Based on this, authors proposed a "bottom-up" mechanism for the formation of monolayer nanosheets. Morpholine, an organic heterocycle compound with a chemical formula of $O(CH_2CH_2)_2NH$, has both amine and ether functional groups. It could provide alkalinity through ionization reaction between its amine groups and water (Fig. 19b). The OH^- released from the hydrolysis reaction of morpholine reacted with metal ions, forming Co–Ni LDH. The rapid and complete consumption of water from $Ni(NO_3)_2\cdot 6H_2O$ and $Co(NO_3)_2\cdot 6H_2O$ impeded the formation of hydrogen-bonding of interlayers (Fig. 19b), the monolayer nanosheets were obtained.

Exfoliation of LDH into nanosheets typically consists of two steps: (1) LDH were prepared by different methods; (2) intercalation of large molecules to increase the interlayer distance. Mechanical agitation to drive exfoliation and exfoliation without any solvent are adopted in the exfoliation process. Direct synthesis of LDH monolayer nanosheets mainly focused on controlling the nucleation and growth conditions. Different LDH exfoliation methods/direct growth methods are summarized in Table 1.

3 Practical applications of LDH nanosheets

The applications of LDH nanosheets have been extensively studied and continues to expand. Currently, the LDH nanosheets have been used in many fields. In this section, we mainly summarize the application of LDH nanosheets in the four fields: (1) as catalysts for the oxygen evolution reaction, (2) as crosslinkers for the polymer composites, (3) as constructing materials for supercapacitors, (4) as carriers for drugs.

3.1 Catalysts

In recent years, the LDH nanosheets as catalysts for the reaction of oxygen evolution from water has been widely studied.[54,72–96] Zhang *et al.*[93] reported the preparation of porous monolayer NiFe-LDH (PM-LDH) by a facile one-step strategy, which can be used as an outstanding electrocatalyst for the oxygen evolution reaction (OER) (Fig. 20). The prepared PM-LDH showed an excellent OER electrocatalytic activity with an overpotential as low as 230 mV at a current density of 10 mA cm^{-2} and a Tafel slope of only 47 mV dec^{-1}. Moreover, the OER activity could be maintained for a 100 h test period if the electrolyte was

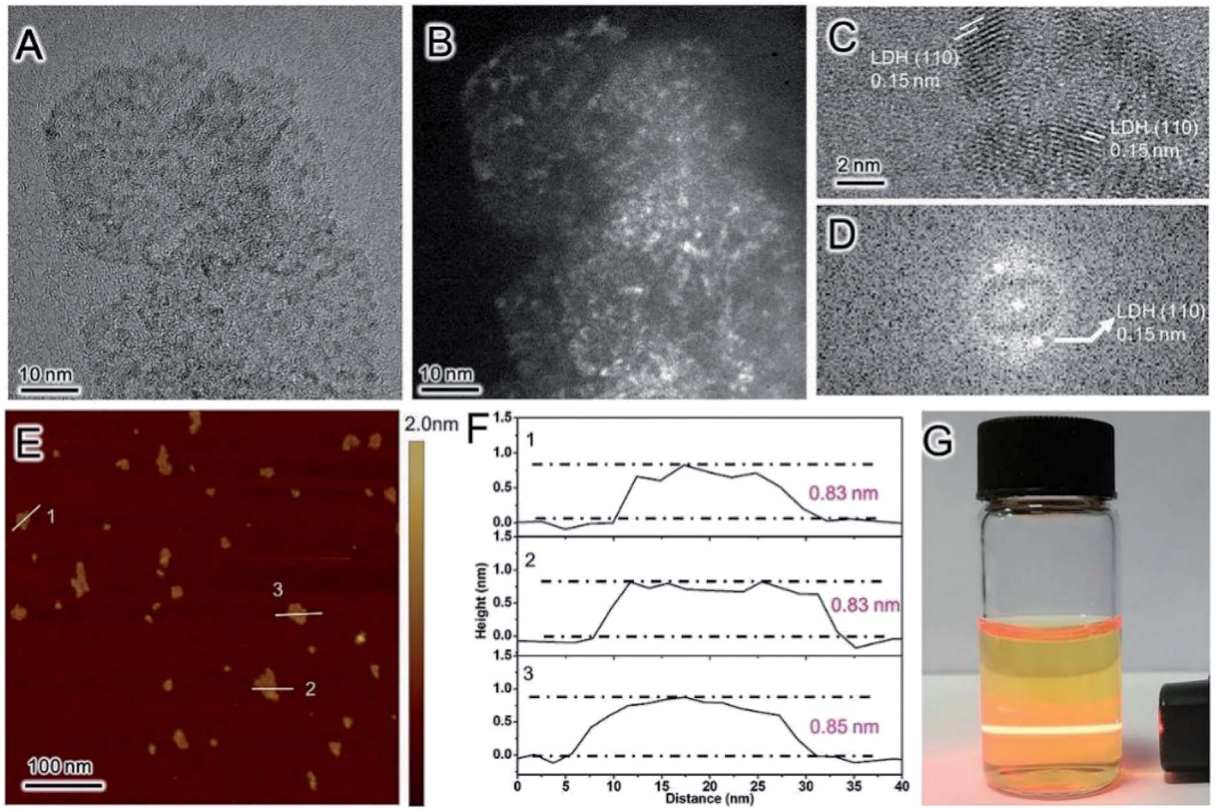

Fig. 20 (A) TEM, (B) HAADF-STEM, and (C) HRTEM image of PM-LDH; (D) the FFT pattern of the image shown in (C). (E) AFM image and (F) AFM height profiles of PM-LDH; the numbers 1–3 in (E) correspond to the profiles 1–3 in (F). (G) A dispersion of PM-LDH in ethanol displaying the Tyndall effect. Reproduced with permission from ref. 93. Copyright 2019 John Wiley & Sons, Inc.

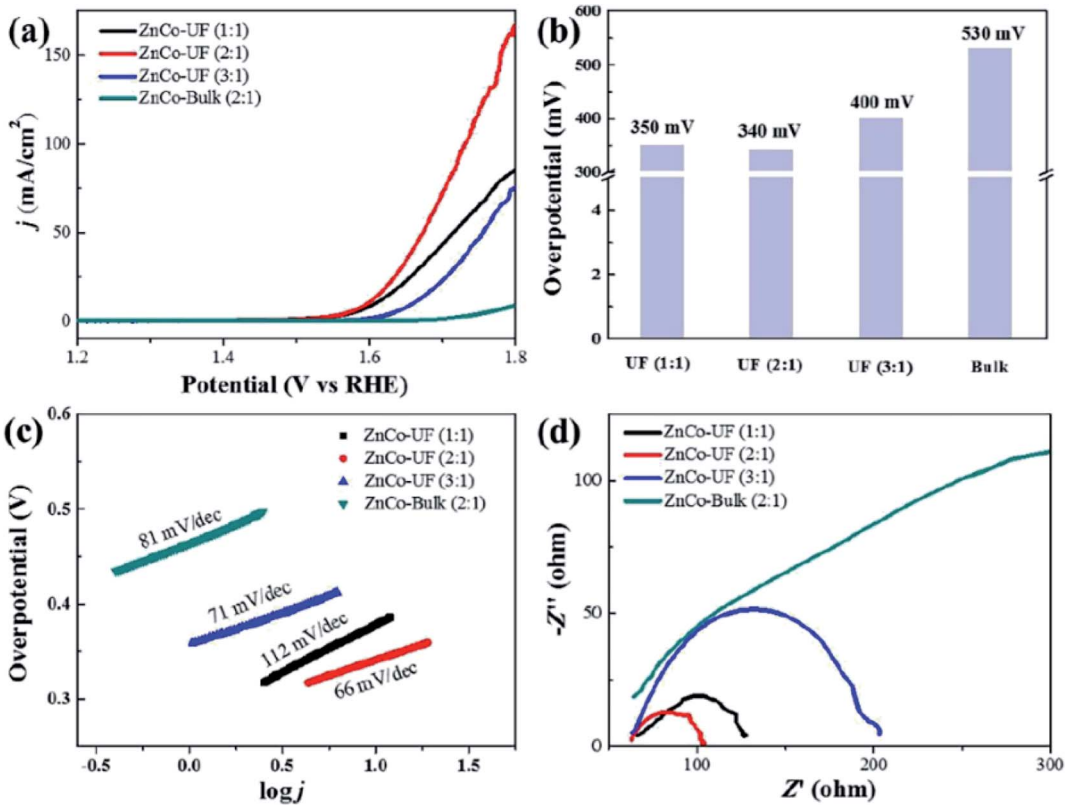

Fig. 21 (a) LSV curves for OER measured at a scan rate of 5 mV s^{-1}; (b) the overpotential of ZnCo-UF at the current density of 5 mA cm^{-2}; (c) corresponding Tafel plots; (d) EIS Nyquist plots at 1.8 V. Reproduced with permission from ref. 94. Copyright 2019 Elsevier Inc.

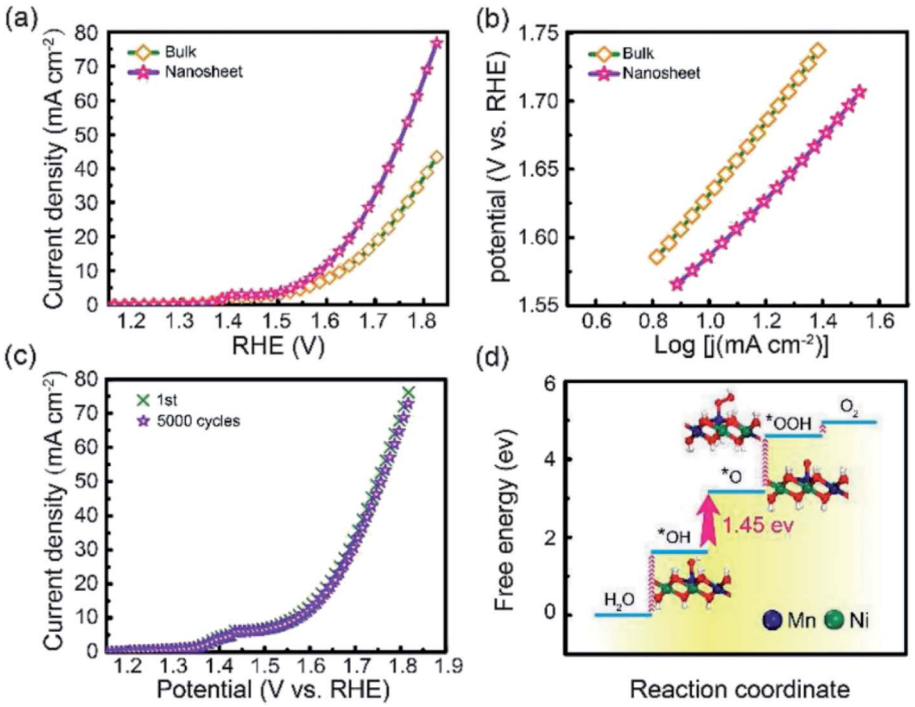

Fig. 22 (a) LSV curves for OER on bulk NiMn-LDH and ultrathin NiMn-LDH nanosheets. (b) The corresponding Tafel plots. (c) Cycles stability of the exfoliated NiMn-LDH nanosheets. (d) DFT calculated free energy diagrams for the OER process from H_2O to O_2 on the NiMn-LDH structures. The optimized configurations of the adsorption intermediates of *OH, *O and *OOH are shown inside. Dark blue: Mn; green: Ni; red: O; white: H. Reproduced with permission from ref. 95. Copyright 2018 John Wiley & Sons, Inc.

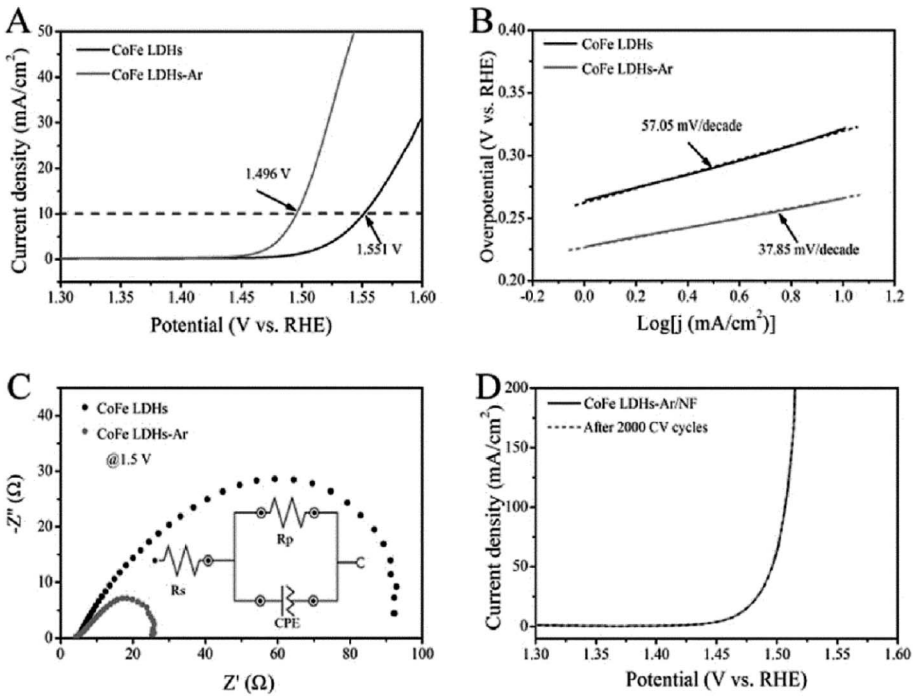

Fig. 23 The OER performance of bulk CoFe LDH and ultrathin CoFe LDH-Ar nanosheets. (A) LSV curves for the OER at a scan rate of 5 mV s^{-1}. (B) The corresponding Tafel plots. (C) Nyquist plots at an overpotential of 270 mV. The inset gives the equivalent circuit. R_s = series resistance, R_p = charge transfer resistance, CPE = constant phase element related to the double-layer capacitance. (D) Stability test with the CoFe LDH-Ar on Ni foam. Reproduced with permission from ref. 54. Copyright 2017 John Wiley & Sons, Inc.

Table 2 Tensile and compressive mechanical properties of the hydrogels, including the as-prepared ones (PAM, L_mM, B_nM) (the conventional chemically crosslinked hydrogels using *N,N,N′,N′*-methylenebis(acrylamide) as the crosslinker, where *n* represents 3 × BIS/water [g L^{-1}]) and the swollen one with 90 wt% water content (L_2M-S)

Sample	Yield strength [kPa]	Fracture strength [kPa]	Elongation at break [%]	Toughness[a] [MJ m^{-3}]	Compressive strength[b] [MPa]	Compressive modulus[b] [MPa]
L_1M	39.5	29.3	2355	0.69 0.5	4.5	
L_2M	58.4	43.2	4068	1.99	0.9	12.9
L_3M	62.3	45.8	4361	2.55	1.2	16.6
L_2M-S[c]	No	>34.0	>6236	>1.95		
B_1M	—	41.4	318	0.10	—	—
B_2M	—	59.3	204	0.08	—	—
PAM	21.7	7.0	154	0.02	—	—

[a] Toughness was calculated from the areas under the tensile stress–strain curves. [b] The hydrogels B1M, B2M, and PAM were too brittle to compress. [c] The swollen hydrogel L2M-S did not break during the tensile test, accompanied by the disappearance of the yielding phenomenon.

refreshed every 20 h, and the faradaic efficiency of the PM-LDH was of ≈100% over 30 min, representing one of the best OER performance yet reported for a NiFe-LDH system.

Jia *et al.*[94] studied the OER activity of ultrafine monolayer Zn_n/Co_k–LDH (ZnCo-UF) nanosheets (with $n:k$ molar ratios of 1 : 1, 2 : 1 or 3 : 1), ZnCo-UF nanosheets were synthesized by exfoliating the bulk Zn_n/Co_k–LDH (ZnCo-bulk) in formamide. The prepared ZnCo-UF with a mean size of ∼3.5 nm and thickness of ∼0.5 nm were tested as a catalyst for OER reactions (Fig. 21). ZnCo-UF (2 : 1) exhibited outstanding OER activity compared with ZnCo-bulk, with the current density of 168 mA cm^{-2} almost 20 times higher than that of ZnCo-bulk (8.5 mA cm^{-2}) under a potential at 1.8 V. Moreover, comparing with ZnCo-UF prepared at Zn : Co ratios of 1 : 1 and 3 : 1, ZnCo-UF (2 : 1) displayed superior performance with a lower overpotential for OER, higher current density and the lowest OER Tafel slope of 66 mV dec^{-1}. The prepared ZnCo-UF were active for hydrogen evolution reactions. The high current density, low OER overpotential, small charge transfer resistance and large eletroactive surface area make ZnCo-UF (2 : 1) an excellent electrocatalyst for OER.

Li *et al.*[95] studied the OER activity of ultrathin NiMn-LDH nanosheets synthesized by a one-step method with the assistance of ultrasonication at room temperature. The prepared NiMn-LDH nanosheets and the bulk NiMn-LDH synthesized by a typical coprecipitation method were tested as a catalyst for

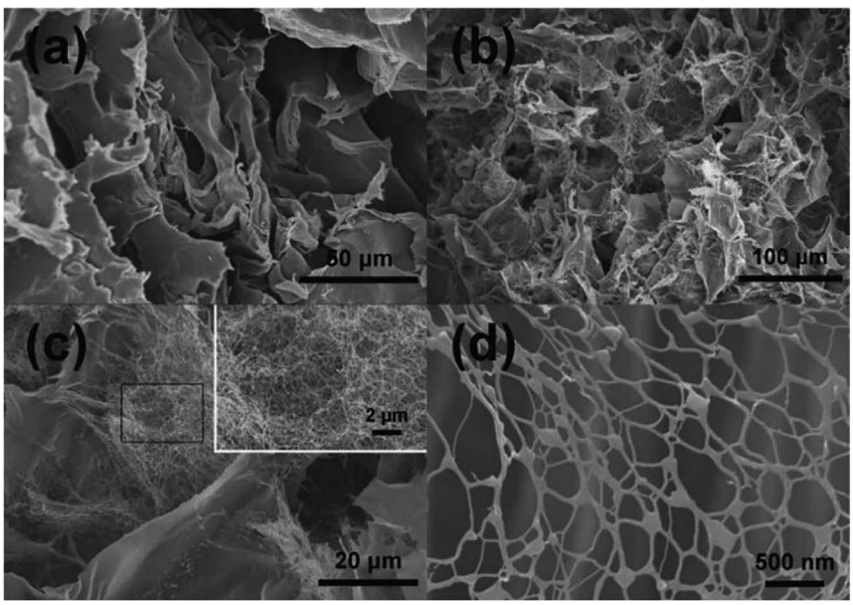

Fig. 24 Typical SEM images of the freeze-dried xerogels for the neat PAM hydrogel (a) and the LDH/PAM NC hydrogel (L_1M) (b–d). The neat PAM xerogel showed the common large-pore structure at the micrometer scale (a). In contrast, the NC xerogel revealed an unusual hierarchical porous structure with interconnected pore sizes at micro- and nanometer scales (b and c). Inset in (c): enlargement of the outlined rectangular part. (d) Details of the nanometer-sized pores. Reproduced with permission from ref. 97. Copyright 2014 John Wiley & Sons, Inc.

Table 3 Tensile and compression mechanical properties of the LDH/PAM NC hydrogels (L_mM)

Sample	Yield strength (kPa)	Fracture strength (kPa)	Elongation at break (%)	Tensile modulus (kPa)	Toughness[a] (MJ m^{-3})	N^* (mol m^{-3})	10^4 M_c (g mol^{-1})	Compressive strength (MPa)	Compressive modulus (kPa)
L_1M	20.9	21.0	3800	36.4	0.64	10.7	9.38	0.43	53.7
L_2M	21.7	>33.4	>3950	32.1	0.83	9.99	10.0	0.69	66.9
L_3M	26.6	>67.0	>4936	39.5	1.70	11.2	8.96	1.02	78.3

[a] Toughness was calculated from the areas under the tensile stress–strain curves.

OER reactions (Fig. 22). Compared with the bulk NiMn-LDH, the as obtained NiMn-LDH nanosheets exhibited a twofold enhancement of the activity and a reduction of overpotential by 80 mV at 10 mA cm^{-2}. The Tafel slope of the as-prepared NiMn-LDH nanosheets and bulk NiMn-LDH material was of ≈47 and 93 mV dec^{-1}, respectively.

Wang *et al.*[54] reported the preparation of ultrathin CoFe LDH nanosheets obtained by dry exfoliation in Ar plasma (CoFe LDH-Ar). The obtained CoFe LDH-Ar with multiple vacancies was an excellent electrocatalyst for the OER (Fig. 23). The CoFe LDH-Ar exhibited higher OER activity with a lower overpotential of 266 mV at 10 mA cm^{-2} than the bulk CoFe LDH (321 mV at 10 mA cm^{-2}). And the CoFe LDH-Ar exhibited a smaller Tafel slope of 37.85 mV per decade than the bulk CoFe LDH (57.05 mV per decade). Furthermore, after loading the CoFe LDH-Ar onto nickel foam (denoted as CoFe LDH-Ar/NF) with a loading capacity of 0.2 mg cm^{-2}, the obtained CoFe LDH-Ar/NF had an ultralow overpotential of 237 mV at a current density of 10 mA cm^{-2}. And the LSV curve of CoFe LDH-Ar/NF for the OER showed negligible degradation after 2000 CV cycles, indicating a superior operational stability of the CoFe LDH-Ar.

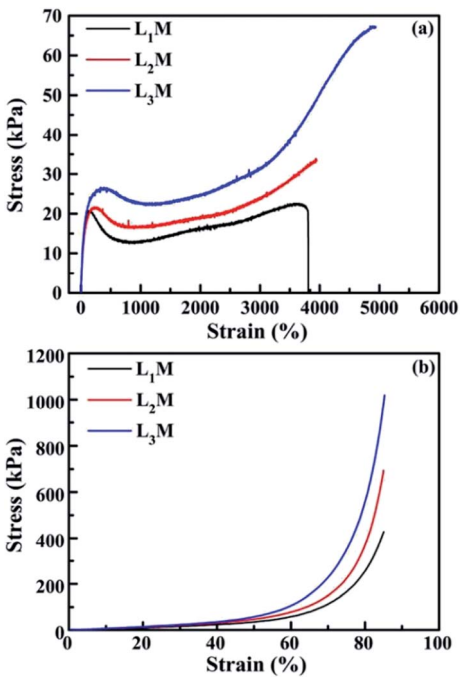

Fig. 25 Stress–strain curves of (a) tensile and (b) compression measurements for the as-prepared LDH/PAM NC hydrogels (L_mM). Reproduced with permission from ref. 98. Copyright 2015 The Royal Society of Chemistry.

3.2 Nanocrosslinker

Due to their highly flexible and tunable chemical composition and excellent physical properties, LDH have found widespread applications in LDH/polymer nanocomposites (NC).[97–103] Well dispersed LDH nanosheets in polymer matrices can greatly improve the mechanical and water-swelling properties. For example, Hu *et al.*[97] reported a novel type of polymer NC hydrogels, LDH/polyacrylamide (PAM), prepared by means of a convenient *in situ* polymerization method. The obtained LDH/polymer NC hydrogels exhibited ultrahigh tensibility and excellent toughness even at low inorganic content (≤2.3 wt%), as well as unusual hierarchical porous structure, as shown in Table 2 and Fig. 24. In addition, with the increase of isethionate ($HO(CH_2)_2SO_3^-$)-intercalated LDH (LDH-Ise) content, the compression strengths and moduli of the LDH/PAM NC hydrogels (L_mM, where m stands for the concentration 0.1 × LDH/water [g L^{-1}]) increased significantly. This type of LDH/polymer NC hydrogels may further widen the applications of polymer hydrogels in mechanical devices such as biomedical devices, artificial muscles, and drug delivery systems.

Wu *et al.*[98] developed a convenient green preparation method to achieve LDH/polyacrylamide (PAM) NC hydrogels with ultrahigh deformability. The ZnAl-LDH with amino acid (L-Ser) were first delaminated in water resulting in a transparent aqueous dispersion, then the monomer, initiator and accelerator were dissolved under stirring at 0 °C for 10 min. Subsequently, NC hydrogels were achieved *via* exfoliation–adsorption *in situ* polymerization. The prepared NC hydrogels exhibited ultrahigh deformability towards various mechanical deformations including elongation, bending, knotting, knotting and subsequent elongation, and compression. Additionally, the NC hydrogels displayed extraordinary stretchability and compressibility as shown in Table 3 and Fig. 25.

Huang *et al.*[99] reported the facile preparation of bioactive nanocomposite PEG hydrogel crosslinked by the novel multifunctional nanocrosslinkers, polydopamine-coated LDH (PD-LDH). Fig. 26 illustrates the synthesize process, in which the LDH nanosheets were first coated by polydopamine, then the PD-LDH nanosheets were mixed with the commercially

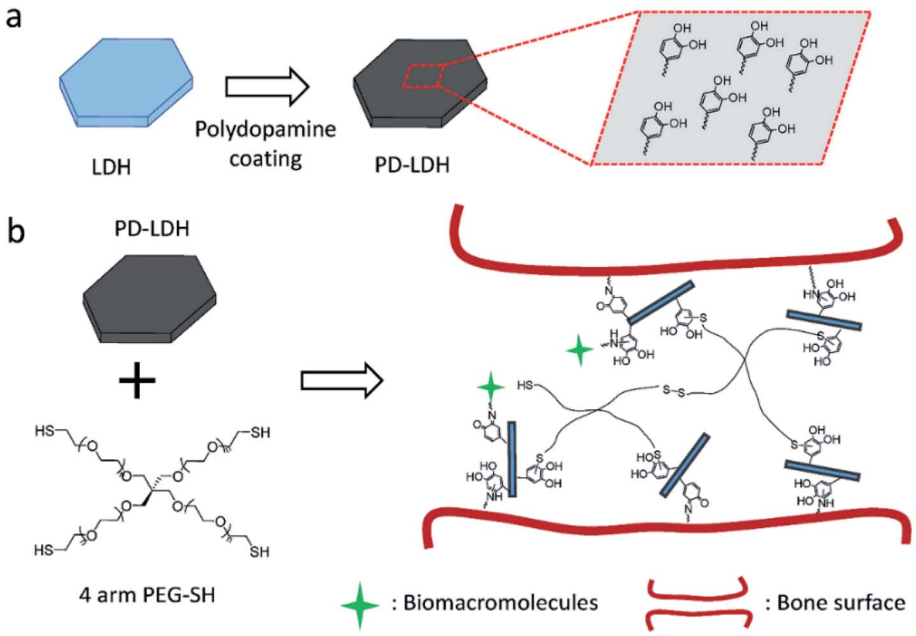

Fig. 26 (a) Schematic representation of polydopamine coating on layered double hydroxides (LDH). (b) Schematic of nanocomposite hydrogel synthesized with 4 arm thiol-terminated polyethylene glycol (4 arm PEG-SH) and polydopamine-coated LDH (PD-LDH), which is able to immobilize biomacromolecules and act as the bioadhesive for bone fracture. Reproduced with permission from ref. 99. Copyright 2016 John Wiley & Sons, Inc.

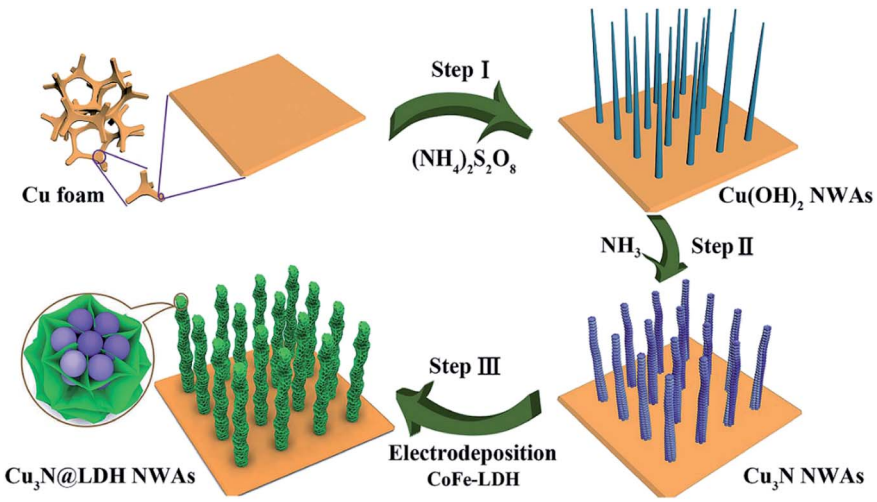

Fig. 27 Schematic illustration for the fabrication of hierarchical Cu_3N@CoFe-LDH core–shell NWAs supported on copper foam. Reproduced with permission from ref. 128. Copyright 2018 The Royal Society of Chemistry.

available 4 arm thiol terminated polyethylene glycol (4 arm PEG-SH) to form poly(ethylene glycol) (PEG) hydrogels. Acting as nanocrosslinkers, the catechol-rich PD-LDH nanosheets reinforced the mechanical strength of the hydrogel as well as afforded the hydrogels with bioadhesion and robust bioactivity by the cortical-mediated couplings. The prepared nanocomposite PEG hydrogels exhibited tunable mechanical properties, self-healing ability, and bioadhesion to biological tissues. Moreover, without any further bio-functionalization these hydrogels could promote the sequestration of proteins and support the osteogenic differentiation of human mesenchymal stem cells.

3.3 Supercapacitors

In recent years, due to the structural tunability, LDH as metal oxide precursors or the source of pseudo-capacitive species have attracted increasing attention in supercapacitor research.[104–130] For example, a novel three-dimensional (3D) embedded hierarchical core–shell nanostructure was developed *via* combining ultrathin CoFe-LDH nanosheets with porous Cu_3N nanowire

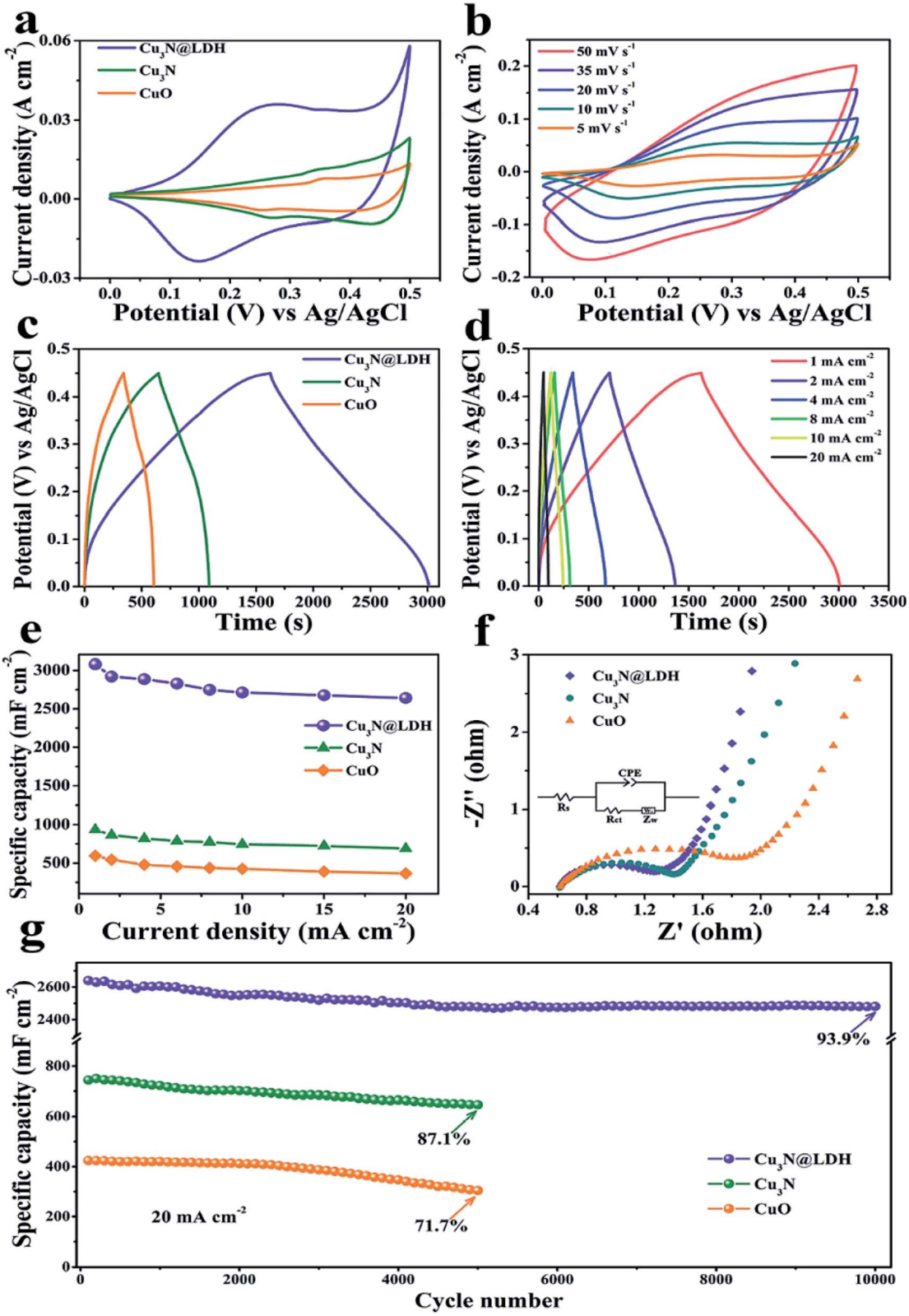

Fig. 28 (a) CV curves of CuO, Cu_3N and Cu_3N@CoFe-LDH at a scan rate of 5 mV s^{-1}. (b) CV curves of Cu_3N@CoFe-LDH at various scan rates. (c) GCD curves of CuO, Cu_3N and Cu_3N@CoFe-LDH at a current density of 1 mA cm^{-2}. (d) GCD curves of Cu_3N@CoFe-LDH at various current densities. (e) Current density dependence of the areal capacitance, (f) Nyquist plots of EIS and (g) cycling performance of the pristine CuO, Cu_3N and Cu_3N@CoFe-LDH. Reproduced with permission from ref. 128. Copyright 2018 The Royal Society of Chemistry.

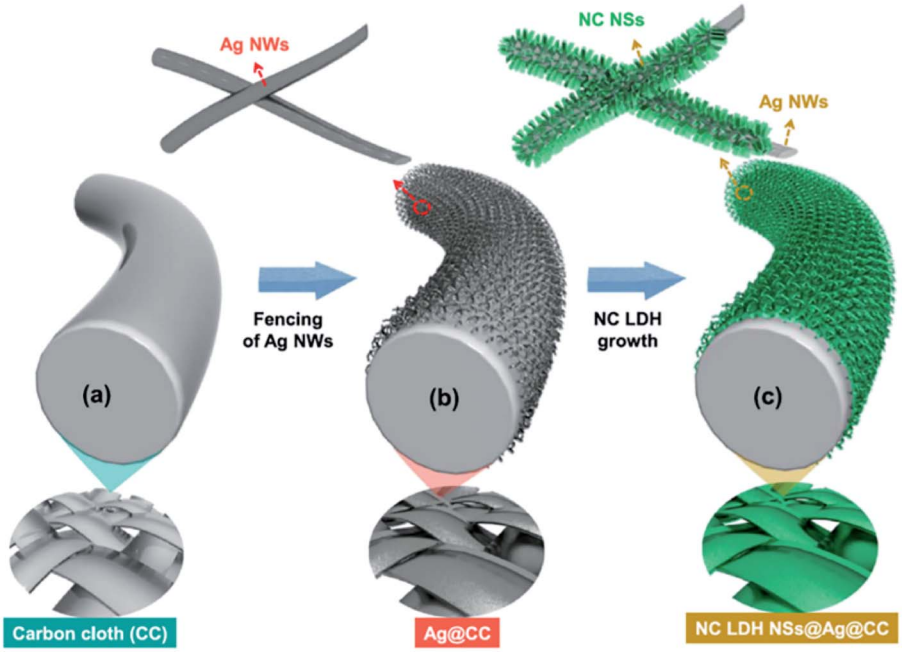

Fig. 29 (a–c) Schematic illustration showing the preparation process flow of NC LDH NSs@Ag@CC by a single-step ECD process. Reproduced with permission from ref. 129. Copyright 2017 Elsevier Inc.

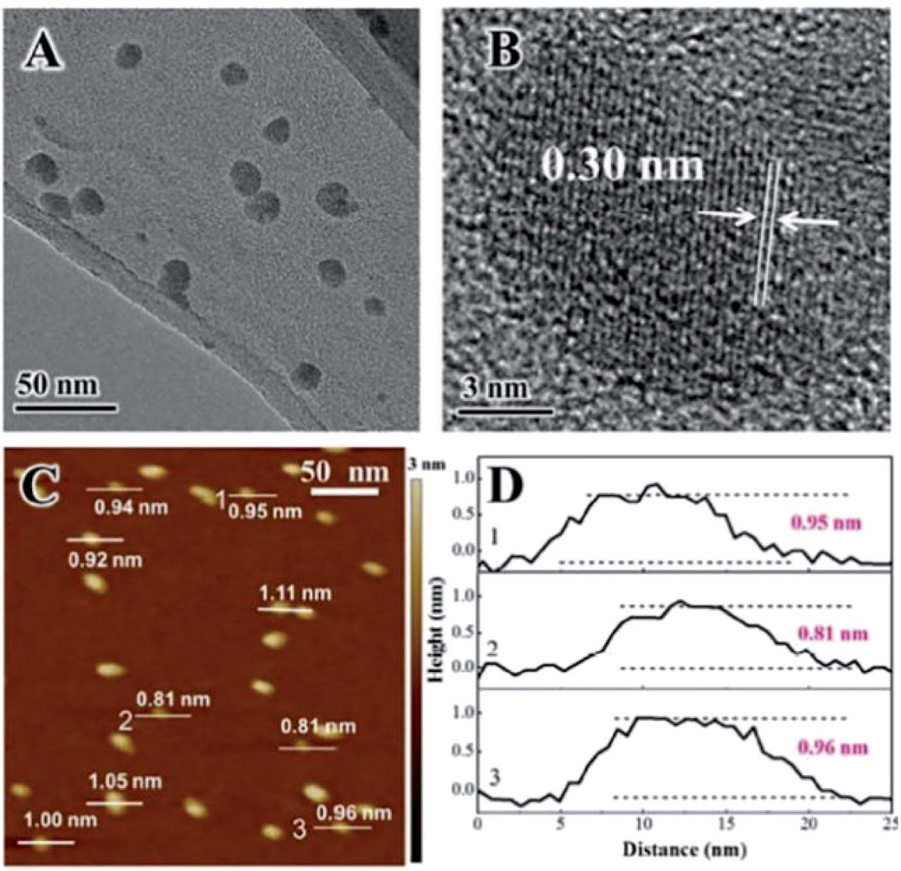

Fig. 30 Characterizations for the monolayer-NiTi-LDH nanosheets. (A) TEM image; (B) HRTEM image; (C) AFM image and (D) the corresponding height profiles; the numbers from 1 to 3 in (D) correspond to the numbers from 1 to 3 in (C). Reproduced with permission from ref. 130. Copyright 2015 The Royal Society of Chemistry.

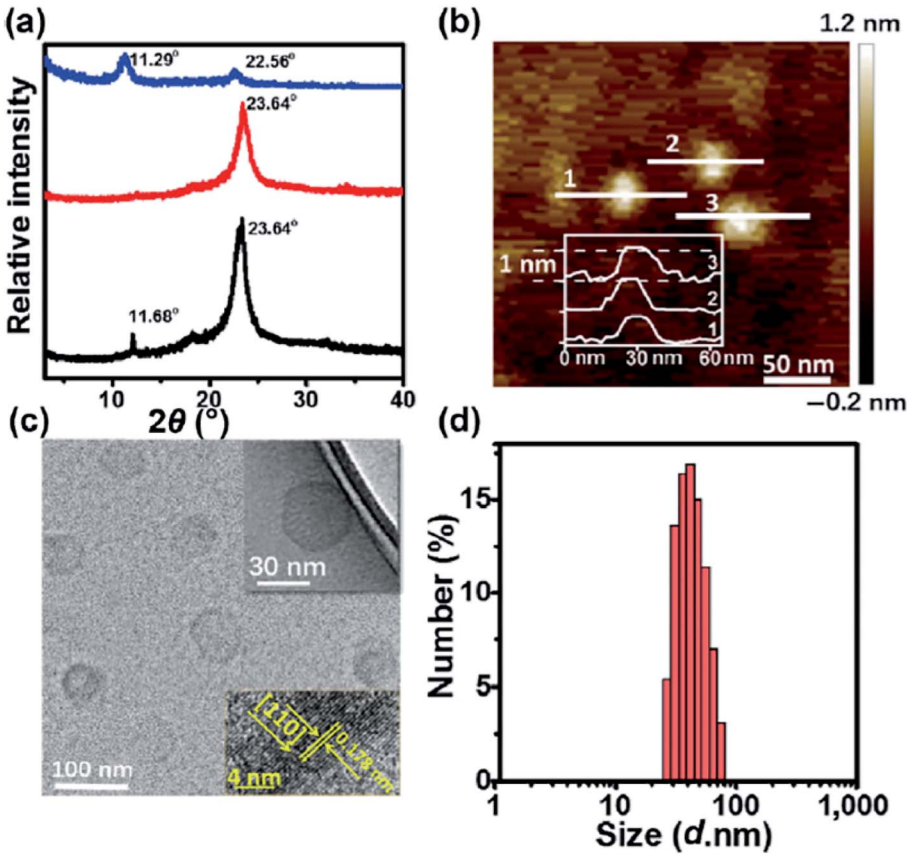

Fig. 31 (a) XRD patterns of bulk LDH colloid (black line), MLDH colloid (red line), and the re-stacking of MLDH nanosheets (blue line). (b) AFM image, (c) HRTEM image, and (d) particle size distribution of MLDH nanosheets. The insets in (c) show a high magnification image and crystal lattice. Reproduced with permission from ref. 148. Copyright 2018 Springer.

arrays (NWAs),[128] the ultrathin CoFe-LDH nanosheets in the core–shell nanostructure were grown from the interior of Cu_3N nanowire cores supported on Cu foam (Cu_3N@CoFe-LDH). The synthesis process of the hierarchical Cu_3N@CoFe-LDH core–shell NWAs supported on Cu foam is shown in Fig. 27. The obtained Cu_3N@CoFe-LDH NWA electrode exhibited a high areal capacitance of 3078 mF cm^{-2} at a current density of 1 mA cm^{-2}, superior cycling stability and excellent rate capacity, which is superior to the related CuO@CoFe-LDH NWA electrodes (Fig. 28).

Sekhar *et al.*[129] deposited the binder-free NiCo LDH nanosheets on Ag NWs-fenced carbon cloth (NC LDH NSs@Ag@CC) by a facile electrochemical deposition method (Fig. 29). The obtained hierarchical hybrid nanocomposite led to a relatively high areal capacitance (1133.3 mF cm^{-2} at 1 mA cm^{-2}) and a good cycling stability (80.47% after 2000 cycles) compared to the electrode prepared without Ag NWs. Additionally, a flexible asymmetric supercapacitor (ASC) with NC LDH NSs@Ag@CC as a positive electrode and activated carbon coated CC as a negative electrode was fabricated. The obtained ASC displayed maximum operational potential window of 1.6 V, high areal capacitance of 230.2 mF cm^{-2} and outstanding cycling stability of 88.1% with remarkable energy densities at all the charge–discharge conditions (78.8 μW h cm^{-2} at the power density of 785 μW cm^{-2} and 40 μW h cm^{-2} at the high power density of 12.1 mW cm^{-2}, respectively).

Zhao *et al.*[130] reported that Ni^{3+} doped NiTi-LDH monolayer nanosheets, which were prepared through a facile bottom-up approach, exhibited excellent supercapacitor performances. The monolayer-NiTi-LDH nanosheets had a maximum specific capacitance of 2310 F g^{-1}, much higher than that of bulk NiTi-LDH (377 F g^{-1}) and bulk NiAl-LDH (77 F g^{-1}). Furthermore, the monolayer NiTi-LDH exhibited good cycling performance and excellent rate capability with 82.0% capacitance was remained at a large current density of 12 A g^{-1}. The monolayer NiTi-LDH nanosheets were prepared by an *in situ* growth process in the reverse microemulsion formed by surfactant, co-surfactant and water. Fig. 30 shows the TEM and AFM images of the prepared monolayer NiTi-LDH nanosheets, which confirmed the formation of the monolayer NiTi-LDH nanosheets.

3.4 Drug delivery hosts

Because of their excellent biocompatibility, low toxicity, biodegradable and exchangeable interlayer anion, the LDH have been widely explored as inorganic composite materials for drug/gene delivery.[131–137] However, compared with bulk LDH, monolayer LDH (MLDH) nanosheets exhibit much higher specific surface and more combinative sites, leading to greatly enhanced

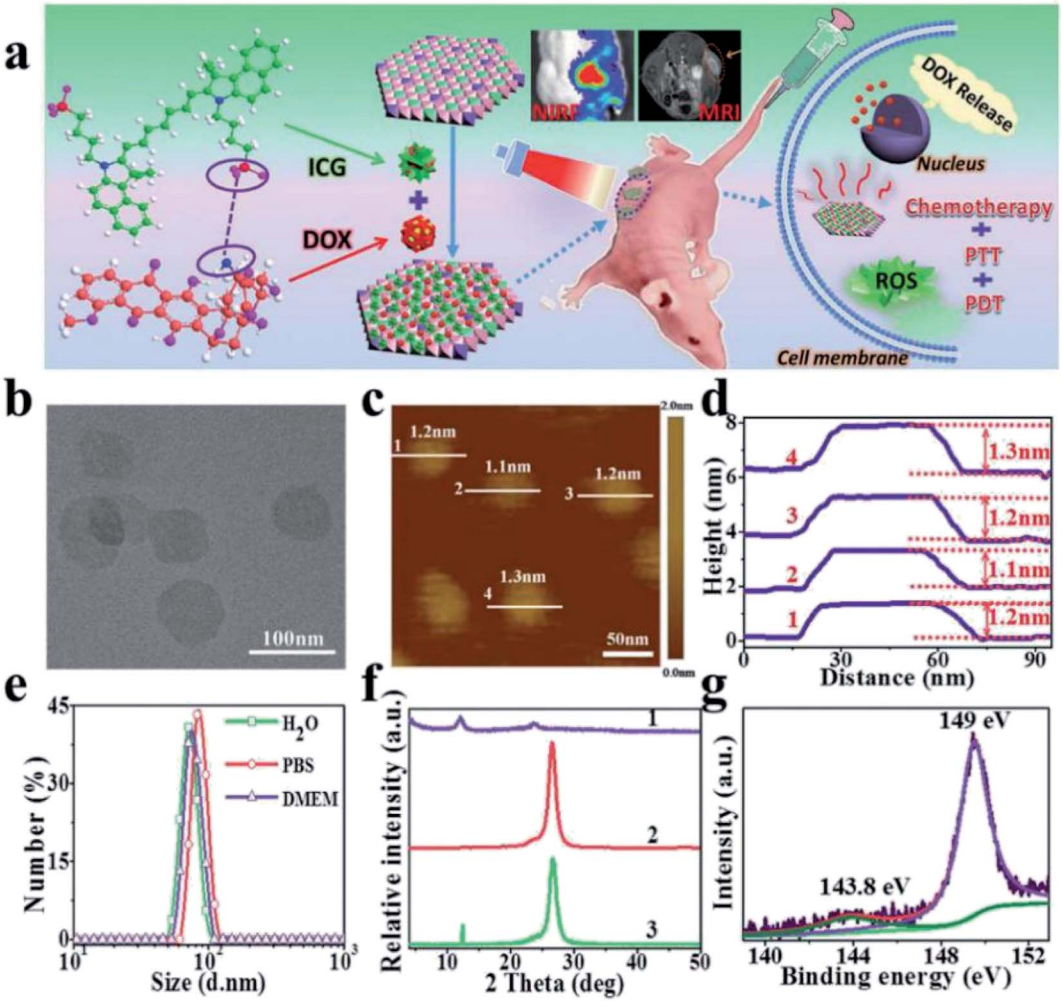

Fig. 32 (a) A schematic illustration for MLDH-based drug delivery system toward efficient loading and precisely controlled delivery of theranostic agents. (b) HRTEM image of MLDH nanosheets. (c) AFM image and (d) measured thickness of MLDH nanosheets. (e) Size distribution of MLDH nanosheets in water, PBS, and culture medium (high glucose Dulbecco's modified Eagle medium (DMEM)). (f) XRD patterns of: (1) bulk LDH colloid, (2) MLDH nanosheets colloid, and (3) the restacking sample of MLDH nanosheets. The peak at 26.2° is ascribed to the PET film substrate. (g) XPS spectra of MLDH nanosheets sample. Reproduced with permission from ref. 149. Copyright 2018 John Wiley & Sons, Inc.

surface activity for drug loading.[138–147] For example, MgAl-LDH monolayer nanosheets were employed to localize doxorubicin (DOX),[148] the DOX/MLDH showed extremely high loading efficiency (3.6 mg mg^{-1} (w/w)) and controllable release behavior. XRD, AFM, and HRTEM confirmed the successful preparation of the MLDH nanosheets (Fig. 31). After further incorporation of folic acid (FA), the as-prepared FA-DOX/MLDH composite showed good fluorescence imaging, selective anticancer performance, and rather low cytotoxicity to normal cells. Moreover, the FA-DOX/MLDH composite exhibited high storage stability, good biocompatibility and targeting capability.

Recently, a Gd^{3+}-doped monolayered-double-hydroxide (MLDH) nanosheets prepared through a bottom-up synthesis procedure as drug carriers was reported.[149] The MLDH nanosheets exhibited ultrahigh drug loading content (LC) of 797.36% and an encapsulation efficiency (EE) of 99.67% towards doxorubicin hydrochloride (DOX) and indocyanine green (ICG) (Fig. 32a). X-ray diffraction (XRD), atomic force microscopy (AFM), high-resolution transmission electron microscopy (HRTEM) and XPS results showed that MLDH nanosheets was successfully synthesized with a uniform lateral size of about 70 nm and a thickness of about 1.2 nm (Fig. 32b–g). The DOX&ICG/MLDH composite exhibited both pH-controlled and near-infrared-irradiation-induced DOX release, resulting in the stimulated drug release performance. Furthermore, the *in vitro* and *in vivo* therapeutic evaluations demonstrated that DOX&ICG/MLDH have excellent trimode synergetic anticancer activity and superior biocompatibility.

Yan *et al.*[150] developed a novel type of aqueous dispersible 2D ultrathin LDH nanosheets and modified their surface with different functional molecules, rhodamine B (RB) and poly(-ethylene glycol) (PEG). After incorporating of rhodamine B, the obtained LDH-Co-RB nanosheets can disperse well in the liquid state, penetrate the cell membrane for bioimaging, and increase intracellular delivery *in vitro*. After tailoring with neutral PEG by covalent bonding, the obtained nanohybrids were suitable for *in vivo* drug delivery through systemic administration. These nanostructures were used for delivery of a negatively charged

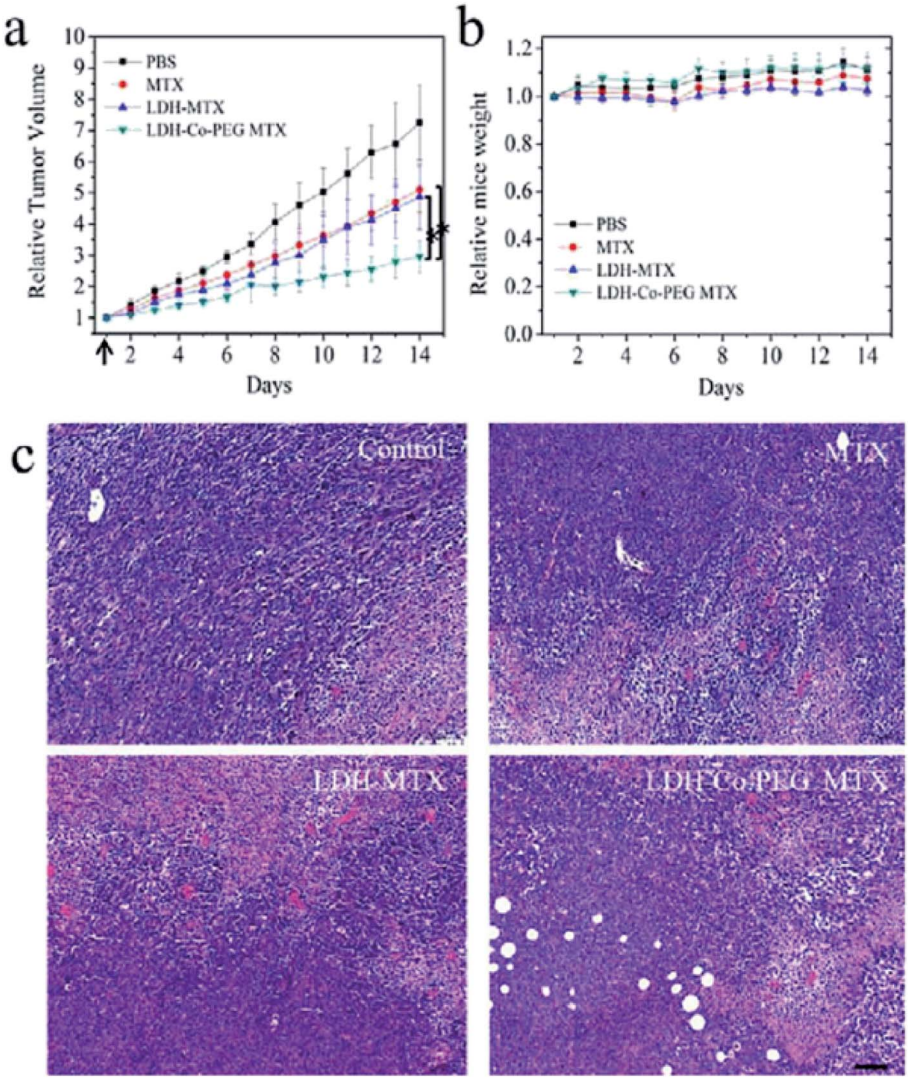

Fig. 33 *In vivo* anticancer activities: (a) tumor growth curves of 4T1 tumor-bearing BALB/C mice after intravenous injection with (1) PBS, (2) free MTX (MTX), (3) MTX loaded in traditional LDH nanoparticles (LDH-MTX), and (4) MTX loaded in PEG-modified ultrathin LDH nanosheets (LDH-Co-PEG MTX) ($n = 5$, error bar indicates standard deviation; the arrow indicates tail vein injection at day 1; * indicates $p < 0.05$ with Student's t test). (b) The body weight evolution of 4T1 tumor-bearing mice at different times after intravenous injection of different materials ($n = 5$, error bar indicates standard deviation). (c) H&E staining images of tumors slices. The tumor-bearing mice were treated with MTX, LDH-MTX, and LDH-Co-PEG MTX at day 1 and sacrificed at day 7. Higher cancer cell damage (red area indicates area of cell damage) was found in LDH MTX- and LDH-Co-PEG MTX-treated groups. Scale bar: 100 μm. Reproduced with permission from ref. 150. Copyright 2017 The American Chemistry Society.

anticancer drug, methotrexate (MTX), and the *in vivo* anticancer therapy results (Fig. 33) showed that MTX loaded in LDH-Co-PEG nanosheets exhibits inhibition of tumor growth significantly better than that of free MTX and MTX loaded in non-modified LDH nanoparticles MTX. In addition, higher cancer cell damage area (red stained) in LDH-MTX- and LDH-Co-PEG MTX-treated groups, indicated dramatically improved therapeutic efficacy was achieved. The further systematic *in vivo* safety investigation demonstrated that the new material was biocompatible.

4 Conclusion and outlook

In this review, we summarized the synthesis methods of LDH nanosheets, including top-down exfoliation methods developed in the recent years and the bottom-up direct synthesis methods. The top-down methods can be realized not only in aqueous solution but also in dry state. The bottom-up approaches are generally achieved by controlling the nucleation and growth conditions so that only allow the formation of dispersed nanosheets. And the bottom-up approaches favors large scale synthesis of dispersible LDH nanosheets.

In recently years, LDH nanosheets were widely applied in many fields, including polymer/LDH nanocomposites, LDH thin films, LDH hybrid magnets, LDH electrode materials, LDH catalysts and bioinorganic hybrid materials. Here, the promising results of LDH catalyzing water splitting reactions, formulating LDH/polymer nanocomposites and supercapacitors, and delivering drugs or genes as carriers were briefly summarized. At present the applications of LDH nanosheets

attracted considerable attention, and many new and significant achievements have been made. However, there are still tough challenges remained to be addressed. In general, the major challenge is how to separate delaminated LDH nanosheets without aggregation from a solvent dispersion. The dispersed LDH nanosheets used in catalyzing water splitting reactions is a very active field over the last several years, LDH nanosheets can work either as support or as the active species. However, in order to obtain most suitable LDH, the exact catalytic mechanism needs to be completely revealed and more major success is anticipated. Fabricating LDH/polymer nanocomposite hydrogels need to overcome the main obstacle: the affinity of LDH with the monomer and the polymer, the surface modification of hydrophilic LDH into hydrophobic ones was needed to maximize their dispersion in polymer matrices. Research into LDH nanosheets in delivery carriers is quite extensive, therefore, its future development should focus on the functionalization of the LDH shells and explore their clinical applications. The study of the LDH nanosheets in supercapacitors is very active, and major progress in this field is anticipated in coming years. In all these applications, the selection of appropriate LDH and the complementary compounds that can deliver the desired multifunctional response is very critical. Proper exfoliation methods need to be choose to optimize the mixing and matching of the two components. Therefore, LDH should be much more attractive prospects in the coming years as they possess unique structure and performance, which remain highly attractive to researchers in chemistry, materials science, and engineering.

Conflicts of interest

The authors declare that they have no known competing financial interests or personal relationships that could have appeared to influence the work reported in this paper.

Acknowledgements

This work was financially supported by the Henan University of Chinese Medicine (No. 00104311-2021-1).

References

1 P. J. Sideris, U. G. Nielsen, Z. H. Gan and C. P. Grey, *Science*, 2008, **321**, 113–117.
2 R. Z. Ma, Z. P. Liu, K. Takada, N. Iyi, Y. Bando and T. Sasaki, *J. Am. Chem. Soc.*, 2007, **129**, 5257–5263.
3 Q. Wang and D. O'Hare, *Chem. Rev.*, 2012, **112**, 4124–4155.
4 Z. P. Liu, R. Z. Ma, Y. Ebina, N. Iyi, K. Takada and T. Sasaki, *Langmuir*, 2007, **23**, 861–867.
5 C. Gomes Silva, Y. Bouizi, V. Fornes and H. Garcia, *J. Am. Chem. Soc.*, 2009, **131**, 13833.
6 J. L. Gunjakar, T. W. Kim, H. N. Kim, I. Y. Kim and S. J. Hwang, *J. Am. Chem. Soc.*, 2011, **133**, 14998.
7 Y. Zhao, M. Wei, J. Lu, Z. L. Wang and X. Duan, *ACS Nano*, 2009, **3**, 4009.
8 K. Parida, M. Satpathy and L. Mohapatra, *J. Mater. Chem.*, 2012, **22**, 7350.
9 H. Nakajima, S. Ishino, H. Masuda, T. Shimosaka, T. Nakagama, T. Hobo and K. Uchiyama, *Chem. Lett.*, 2005, **34**, 358–359.
10 P. Atienzar, M. de Victoria-Rodriguez, O. Juanes, J. C. Rodriguez-Ubis, E. Brunet and H. Garcia, *Energy Environ. Sci.*, 2011, **4**, 4718–4726.
11 J. L. Colon, C. Y. Yang, A. Clearfield and C. R. Martin, *J. Phys. Chem.*, 1990, **94**, 874–882.
12 D. S. Robins and P. K. Dutta, *Langmuir*, 1996, **12**, 402–408.
13 C. P. Chen, P. Gunawan and R. Xu, *J. Mater. Chem.*, 2011, **21**, 1218.
14 Y. Zhao, S. He, M. Wei, D. G. Evans and X. Duan, *Chem. Commun.*, 2010, **46**, 3031.
15 Q. Wang, J. Luo, Z. Zhong and A. Borgna, *Energy Environ. Sci.*, 2011, **4**, 42.
16 Q. Wang, H. H. Tay, Z. Zhong, J. Luo and A. Borgna, *Energy Environ. Sci.*, 2012, **5**, 7526.
17 Q. Wang, H. H. Tay, D. J. W. Ng, L. Chen, Y. Liu, J. Chang, Z. Zhong, J. Luo and A. Borgna, *ChemSusChem*, 2010, **3**, 965.
18 Q. Wang, Z. Wu, H. H. Tay, L. Chen, Y. Liu, J. Chang, Z. Zhong, J. Luo and A. Borgna, *Catal. Today*, 2011, **164**, 198.
19 Q. Wang, H. H. Tay, Z. Guo, L. Chen, Y. Liu, J. Chang, Z. Zhong, J. Luo and A. Borgna, *Appl. Clay Sci.*, 2012, **55**, 18.
20 Q. Wang, H. H. Tay, L. Chen, Y. Liu, J. Chang, Z. Zhong, J. Luo and A. Borgna, *J. Nanoeng. Nanomanuf.*, 2011, **1**, 1.
21 A. C. S. Alcantara, P. Aranda, M. Darder and E. Ruiz-Hitzky, *J. Mater. Chem.*, 2010, **20**, 9495.
22 S. D. Li, J. H. Li, C. J. Wang, Q. Wang, M. Z. Cader, J. Lu, D. G. Evans, X. Duan and D. O'Hare, *J. Mater. Chem. B*, 2013, **1**, 61.
23 Y. Y. Wong, K. Markham, Z. P. Xu, M. Chen, G. Q. Lu, P. F. Bartlett and H. M. Cooper, *Biomaterials*, 2010, **31**, 8770.
24 W. Wang, H. Pan, Y. Shi, Y. Pan, W. Yang, K. Liew, L. Song and Y. Hu, *Composites, Part A*, 2016, **80**, 259–269.
25 H. Pan, W. Wang, Q. Shen, Y. Pan, L. Song, Y. Hu and Y. Lu, *RSC Adv.*, 2016, **6**, 111950.
26 Z. Matusinovic and C. A. Wilkie, *J. Mater. Chem.*, 2012, **22**, 18701–18704.
27 D.-Y. Wang, A. Das, F. R. Costa, A. Leuteritz, Y.-Z. Wang, U. Wagenknecht and G. Heinrich, *Langmuir*, 2010, **26**, 14162–14169.
28 C. Nyambo, P. Songtipya, E. Manias, M. M. Jimenez-Gasco and C. A. Wilkie, *J. Mater. Chem.*, 2008, **18**, 4827.
29 Y. Gao, J. Wu, Q. Wang, C. A. Wilkie and D. O'Hare, *J. Mater. Chem. A*, 2014, **2**, 10996–11016.
30 L. F. Nazar and A. J. Jacobson, *J. Chem. Soc., Chem. Commun.*, 1986, 570–571.
31 N. Yamamoto, T. Okuhara and T. Nakato, *J. Mater. Chem.*, 2001, **11**, 1858.
32 L. F. Nazar, S. W. Liblong and X. T. Yin, *J. Am. Chem. Soc.*, 1991, **113**, 5889.
33 T. Sasaki, M. Watanabe, H. Hashizume, H. Yamada and H. Nakazawa, *J. Am. Chem. Soc.*, 1996, **118**, 8329.
34 R. E. Schaak and T. E. Mallouk, *Chem. Mater.*, 2000, **12**, 2513.

35 R. E. Schaak and T. E. Mallouk, *Chem. Mater.*, 2002, **14**, 1455.
36 S. O'Leary, D. O'Hare and G. Seeley, *Chem. Commun.*, 2002, 1506–1507.
37 F. Song and X. Hu, *Nat. Commun.*, 2014, **5**, 4477.
38 R. Ma and T. Sasaki, *Adv. Mater.*, 2010, **22**, 5082.
39 K. Yan, T. Lafleur, J. J. Chai and C. Jarvis, *Electrochem. Commun.*, 2016, **62**, 24–28.
40 Y. Y. Wang, Y. Q. Zhang, Z. J. Liu, C. Xie, S. Feng, D. D. Liu, M. F. Shao and S. Y. Wang, *Angew. Chem., Int. Ed.*, 2017, **56**, 1–6.
41 K. Fan, H. Chen, Y. F. Ji, H. Huang, P. M. Claesson, Q. Daniel, B. Philippe, H. Rensmo, F. S. Li, Y. Luo and L. C. Sun, *Nat. Commun.*, 2016, **7**, 11981.
42 M. Zubair, M. Daud, G. McKay, F. Shehzad and M. A. Al-Harthi, *Appl. Clay Sci.*, 2017, **143**, 279–292.
43 H. Yin and Z. Tang, *Chem. Soc. Rev.*, 2016, **45**, 4873–4891.
44 J. F. Yu, Q. Wang, D. O'Hare and L. Y. Sun, *Chem. Soc. Rev.*, 2017, **46**, 5950.
45 M. Meyn, K. Beneke and G. Lagaly, *Inorg. Chem.*, 1990, **29**, 5201–5207.
46 J. M. Hidalgo, C. Jimenez-Sanchidrian, M. Mora and J. R. Ruiz, *J. Nanosci. Nanotechnol.*, 2010, **10**, 6562–6566.
47 W. Hou, L. Kang, R. Sun and Z.-H. Liu, *Colloids Surf., A*, 2008, **312**, 92–98.
48 L. J. Chen, B. Sun, X. D. Wang, F. M. Qiao and S. Y. Ai, *J. Mater. Chem. B*, 2013, **1**, 2268–2274.
49 Y. Zhang, H. Y. Sun, X. L. Bai and Y. X. Zhao, *J. Dispersion Sci. Technol.*, 2019, **40**, 811–818.
50 E. G. Lomax, *Amphoteric Surfactants*, CRC Press, New York, 1996.
51 Y. Wei, F. Li and L. Liu, *RSC Adv.*, 2014, **4**, 18044–18051.
52 J. Cai and L. N. Zhang, *Biomacromolecules*, 2006, **7**, 183–189.
53 J. Cai and L. N. Zhang, *Macromol. Biosci.*, 2005, **5**, 539–548.
54 Y. Y. Wang, Y. Q. Zhang, Z. J. Liu, C. Xie, S. Feng, D. D. Liu, M. F. Shao and S. Y. Wang, *Angew. Chem., Int. Ed.*, 2017, **56**, 5867–5871.
55 G. Hu, N. Wang, D. O'Hare and J. Davis, *Chem. Commun.*, 2006, 287–289.
56 A. I. Khan and D. O'Hare, *J. Mater. Chem.*, 2002, **12**, 3191.
57 Z. P. Xu and P. S. Braterman, *J. Mater. Chem.*, 2003, **13**, 268.
58 S. P. Newman and W. Jones, *New J. Chem.*, 1998, **22**, 105–115.
59 F. Bellezza, A. Cipiciani, U. Costantino, M. Nocchetti and T. Posati, *Eur. J. Inorg. Chem.*, 2009, 2603–2611.
60 Y. Yan, Q. Liu, J. Wang, J. Wei, Z. Gao, T. Mann, Z. Li, Y. He, M. Zhang and L. Liu, *J. Colloid Interface Sci.*, 2012, **371**, 15–19.
61 Q. Wang and D. O'Hare, *Chem. Commun.*, 2013, **49**, 6301–6303.
62 J. Yu, B. R. Martin, A. Clearfield, Z. Luo and L. Sun, *Nanoscale*, 2015, **7**, 9448–9451.
63 J. Yu, J. Liu, A. Clearfield, J. E. Sims, M. T. Speiegle, S. L. Suib and L. Sun, *Inorg. Chem.*, 2016, **55**, 12036–12041.
64 H. P. Li, T. N. Tran, B. J. Lee, C. F. Zhang, J. D. Park, T. H. Kang and J. S. Yu, *ACS Appl. Mater. Interfaces*, 2017, **9**, 20294–20298.
65 W. Zhang, Y. Xie, D. Xiong, X. Zeng, Z. Li, M. Wang, Y.-B. Cheng, W. Chen, K. Yan and S. Yang, *ACS Appl. Mater. Interfaces*, 2014, **6**, 9698–9704.
66 G. Xiang, Y.-G. Wang, J. Li, J. Zhuang and X. Wang, *Sci. Rep.*, 2013, **3**, 1411.
67 Q. Zhao, B. Shao, W. Lü, Y. Jia, W. Lv, M. Jiao and H. You, *Cryst. Growth Des.*, 2014, **14**, 1819–1826.
68 T.-B. Hur, T. X. Phuoc and M. K. Chyu, *J. Appl. Phys.*, 2010, **108**, 114312.
69 X. Pang, M. Sun, X. Ma and W. Hou, *J. Solid State Chem.*, 2014, **210**, 111–115.
70 Y. P. Zhang, H. P. Li, N. Du, R. J. Zhang and W. G. Hou, *Colloids Surf., A*, 2016, **501**, 49–54.
71 W. Ma, L. Wang, J. Y. Xue and H. T. Cui, *J. Alloys Compd.*, 2016, **662**, 315–319.
72 H. Liu, Y. Wang, X. Lu, Y. Hu, G. Zhu, R. Chen, L. Ma, H. Zhu, Z. Tie, J. Liu and Z. Jin, *Nano Energy*, 2017, **35**, 350–357.
73 J. Ping, Y. Wang, Q. Lu, B. Chen, J. Chen, Y. Huang, Q. Ma, C. Tan, J. Yang, X. Cao, Z. Wang, J. Wu, Y. Ying and H. Zhang, *Adv. Mater.*, 2016, **28**, 7640–7645.
74 D. Zhao, K. Jiang, Y. Pi and X. Huang, *ChemCatChem*, 2017, **9**, 84–88.
75 R. F. Chong, G. Wang, Y. Q. Du, Y. S. Jia, X. S. Wang, C. Y. Li, Z. X. Chang and L. Zhang, *Chem. Eng. J.*, 2019, **366**, 523–530.
76 F. Song and X. Hu, *J. Am. Chem. Soc.*, 2014, **136**, 16481–16484.
77 Y. Jia, L. Zhang, G. Gao, H. Chen, B. Wang, J. Zhou, M. T. Soo, M. Hong, X. Yan, G. Qian, J. Zou, A. Du and X. Yao, *Adv. Mater.*, 2017, **29**, 1700017.
78 T. S. Munondea, H. T. Zheng and P. N. Nomngongob, *Ultrason. Sonochem.*, 2019, **59**, 104716.
79 Z. Wang, S. Zeng, W. Liu, X. Wang, Q. Li, Z. Zhao and F. Geng, *ACS Appl. Mater. Interfaces*, 2017, **9**, 1488–1495.
80 Y. Wang, Y. Zhang, Z. Liu, C. Xie, S. Feng, D. Liu, M. Shao and S. Wang, *Angew. Chem.*, 2017, **56**, 5867–5872.
81 T. R. Zhan, Y. Sun, Y. J. Wang, W. Cao, X. E. Liu, H. N. Teng and W. G. Hou, *J. Colloid Interface Sci.*, 2019, **552**, 671–677.
82 B. M. Hunter, W. Hieringer, J. R. Winkler, H. B. Gray and A. M. Muller, *Energy Environ. Sci.*, 2016, **9**, 1734–1743.
83 W. Ma, R. Ma, C. Wang, J. Liang, X. Liu, K. Zhou and T. Sasaki, *ACS Nano*, 2015, **9**, 1977–1984.
84 X. L. Yu, J. Q. Liu, W. C. Yin, T. Wang, L. Quan, Y. Ran, J. Y. Cui, L. Wang and Y. H. Zhang, *Appl. Surf. Sci.*, 2019, **492**, 264–271.
85 C. Zhang, J. Zhao, L. Zhou, Z. Li, M. Shao and M. Wei, *J. Mater. Chem. A*, 2016, **4**, 11516–11523.
86 B. Chen, Z. Zhang, S. Kim, S. Lee, J. Lee, W. Kim and K. J. Yong, *ACS Appl. Mater. Interfaces*, 2018, **10**, 44518–44526.
87 K. N. Dinh, P. L. Zheng, Z. F. Dai, Y. Zhang, R. Dangol, Y. Zheng, B. Li, Y. Zong and Q. Y. Yan, *Small*, 2017, 1703257.
88 Y. Y. Wang, D. F. Yan, S. E. Hankari, Y. Q. Zou and S. Y. Wang, *Adv. Sci.*, 2018, **5**, 1800064.
89 Z. L. Wang, S. M. Xu, Y. Q. Xu, L. Tan, X. Wang, Y. F. Zhao, H. H. Duan and Y. F. Song, *Chem. Sci.*, 2019, **10**, 378–384.

90 Y. F. Zhao, X. Zhang, X. D. Jia, G. I. N. Waterhouse, R. Shi, X. R. Zhang, F. Zhan, Y. Tao, L. Z. Wu, C. H. Tung, D. O'Hare and T. R. Zhang, *Adv. Energy Mater.*, 2018, 1703585.
91 Y. Q. Liu, M. Zhang, D. Hu, R. Q. Li, K. Hu and K. Yan, *ACS Appl. Energy Mater.*, 2019, **2**, 1162–1168.
92 Y. Hou, M. R. Lohe, J. Zhang, S. Liu, X. Zhuang and X. Feng, *Energy Environ. Sci.*, 2016, **9**, 478–483.
93 X. Zhang, Y. F. Zhao, Y. X. Zhao, R. Shi, G. I. N. Waterhouse and T. R. Zhang, *Adv. Energy Mater.*, 2019, **9**, 1900881.
94 X. D. Jia, X. Zhang, J. Q. Zhao, Y. F. Zhao, Y. X. Zhao, G. I. N. Waterhouse, R. Shi, L. Z. Wu, C. H. Tung and T. R. Zhang, *J. Energy Chem.*, 2019, **34**, 57–63.
95 R. Q. Li, Y. Q. Liu, H. B. Li, M. Zhang, Y. R. Lu, L. Zhang, J. P. Xiao, F. Boehm and K. Yan, *Small Methods*, 2019, **3**, 1800344.
96 X. Long, J. Li, S. Xiao, K. Yan, Z. Wang, H. Chen and S. Yang, *Angew. Chem., Int. Ed.*, 2014, **53**, 7584–7588.
97 Z. Q. Hu and G. M. Chen, *Adv. Mater.*, 2014, **26**, 5950–5956.
98 L. Y. Wu, Z. Q. Hu, G. M. Chen and Z. B. Li, *Soft Matter*, 2015, **11**, 9038–9044.
99 H. Q. Huang, J. B. Xu, K. C. Wei, Y. J. Xu, C. K. K. Choi, M. L. Zhu and L. M. Bian, *Macromol. Biosci.*, 2016, **16**, 1019–1026.
100 Z. Q. Hu and G. G. Chen, *RSC Adv.*, 2013, **3**, 12021–12025.
101 N. J. M. Sebri, A. F. A. Latip, R. Adnan, M. H. Hussin and T. Kobayashi, *J. Appl. Polym. Sci.*, 2020, **137**, 48637.
102 X. J. Yang, P. Zhang, P. Li, Z. T. Li, W. Xia, H. Y. Zhang, Z. G. Di, M. L. Wang, H. Q. Zhang and Q. S. J. Niu, *J. Mol. Liq.*, 2019, **280**, 128–134.
103 Y. P. Zhang, J. W. Ji, H. P. Li and W. G. Hou, *Soft Matter*, 2018, **14**, 1789.
104 D. Zha, H. Sun, Y. Fu, X. Ouyang and X. Wang, *Electrochim. Acta*, 2017, **236**, 18–27.
105 X. Li, J. Zai, Y. Liu, X. He, S. Xiang, Z. Ma and X. Qian, *J. Power Sources*, 2016, **325**, 675–681.
106 F. Lai, Y.-E. Miao, L. Zuo, H. Lu, Y. Huang and T. Liu, *Small*, 2016, **12**, 3235–3244.
107 G. Nagaraju, G. S. R. Raju, Y. H. Ko and J. S. Yu, *Nanoscale*, 2016, **8**, 812–825.
108 F. Gu, X. Cheng, S. Wang, X. Wang and P. S. Lee, *Small*, 2015, **11**, 2044–2050.
109 X. Wang, X. Li, X. Du, X. Ma, X. Hao, C. Xue, H. Zhu and S. Li, *Electroanalysis*, 2017, **29**, 1–9.
110 J. Wu, W.-W. Liu, Y.-X. Wu, T.-C. Wei, D. Geng, J. Mei, H. Liu, W.-M. Lau and L.-M. Liu, *Electrochim. Acta*, 2016, **203**, 21–29.
111 H. N. Xing, Y. Y. Lan, Y. Zong, Y. Sun, X. H. Zhu, X. H. Li and X. L. Zheng, *Inorg. Chem. Commun.*, 2019, **101**, 125–129.
112 X. L. Guo, X. Y. Liu, X. D. Hao, S. J. Zhu, F. Dong, Z. Q. Wen and Y. X. Zhang, *Electrochim. Acta*, 2016, **194**, 179–186.
113 R. Zhang, H. An, Z. Li, M. Shao, J. Han and M. Wei, *Chem. Eng. J.*, 2016, **289**, 85–92.
114 F. Lai, Y. Huang, Y.-E. Miao and T. Liu, *Electrochim. Acta*, 2015, **174**, 456–463.
115 M. Li, J. Cheng, J. Wang, F. Liu and X. Zhang, *Electrochim. Acta*, 2016, **206**, 108–115.
116 X. Y. Gao, Y. F. Zhao, K. Q. Dai, J. T. Wang, B. Zhang and X. J. Shen, *Chem. Eng. J.*, 2020, **384**, 123373.
117 X. Wang, Y. Zheng, J. Yuan, J. Shen, J. Hu, A.-J. Wang, L. Wu and L. Niu, *Electrochim. Acta*, 2017, **224**, 628–635.
118 F. Lai, Y. E. Miao, L. Zuo, H. Lu, Y. Huang and T. Liu, *Small*, 2016, **12**, 3199.
119 C. Wang, X. Zhang, X. Sun and Y. Ma, *Electrochim. Acta*, 2016, **191**, 329–336.
120 R. Ma, X. Liu, J. Liang, Y. Bando and T. Sasaki, *Adv. Mater.*, 2014, **26**, 4173–4178.
121 Y. L. Li, L. N. Shan, Y. W. Sui, J. Q. Qi, F. X. Wei, Y. Z. He, Q. K. Meng, Y. J. Ren and J. L. Liu, *J. Mater. Sci.: Mater. Electron.*, 2019, **30**, 13360–13371.
122 K. Ma, J. Cheng, J. Zhang, M. Li, F. Liu and X. Zhang, *Electrochim. Acta*, 2016, **198**, 231–240.
123 Z. Huang, S. Wang, J. Wang, Y. Yu, J. Wen and R. Li, *Electrochim. Acta*, 2015, **152**, 117–125.
124 T. Wang, S. Zhang, X. Yan, M. Lyu, L. Wang, J. Bell and H. Wang, *ACS Appl. Mater. Interfaces*, 2017, **9**, 15510–15524.
125 Z. Yang, X. M. Wang, H. Zhang, S. H. Yan, C. Zhang and S. X. Liu, *ChemElectroChem*, 2019, **6**, 4456–4463.
126 J. Zhao, J. Chen, S. Xu, M. Shao, Q. Zhang, F. Wei, J. Ma, M. Wei, D. G. Evans and X. Duan, *Adv. Funct. Mater.*, 2014, **24**, 2938–2946.
127 H. Chen, L. Hu, M. Chen, Y. Yan and L. Wu, *Adv. Funct. Mater.*, 2014, **24**, 934–942.
128 X. Zhou, X. H. Li, D. J. Chen, D. Y. Zhao and X. T. Huang, *J. Mater. Chem. A*, 2018, **6**, 24603–24613.
129 S. C. Sekhar, G. Nagaraju and J. S. Yu, *Nano Energy*, 2017, **36**, 58–67.
130 Y. F. Zhao, Q. Wang, T. Bian, H. J. Yu, H. Fan, C. Zhou, L. Z. Wu, C. H. Tung, D. O'Harec and T. R. Zhang, *Nanoscale*, 2015, **7**, 7168–7173.
131 L. Li, W. Y. Gu, J. Liu, S. Y. Yan and Z. P. Xu, *Nano Res.*, 2015, **8**, 682–694.
132 J.-H. Choy, S.-Y. Kwak, J.-S. Park, Y.-J. Jeong and J. Portier, *J. Am. Chem. Soc.*, 1999, **121**, 1399–1400.
133 Z. L. Liu, D. Y. Tian, S. P. Li, X. D. Li and T. H. Lu, *Int. J. Pharm.*, 2014, **473**, 414–425.
134 L. Li, W. Y. Gu, J. Z. Chen, W. Y. Chen and Z. P. Xu, *Biomaterials*, 2014, **35**, 3331–3339.
135 D. H. Park, J. E. Kim, J. M. Oh, Y. G. Shul and J. H. Choy, *J. Am. Chem. Soc.*, 2010, **132**, 16735–16736.
136 S. Bégu, A. Aubert-Pouëssel, R. Polexe, E. Leitmanova, D. A. Lerner, J.-M. Devoisselle and D. Tichit, *Chem. Mater.*, 2009, **21**, 2679–2687.
137 R. Z. Liang, R. Tian, L. N. Ma, L. L. Zhang, Y. L. Hu, J. Wang, M. Wei, D. Yan, D. G. Evans and X. Duan, *Adv. Funct. Mater.*, 2014, **24**, 3144–3151.
138 Y. Li, H. Y. Bi, G. W. Wang, N. Wang, C. X. Chen, Z. Z. Li and X. M. Fan, *J. Dispersion Sci. Technol.*, 2016, **37**, 366–373.
139 L. Li, Z. Gu, W. Y. Gu and Z. P. Xu, *RSC Adv.*, 2016, **6**, 95518.
140 Y. Li, W. L. Bao, H. Y. Wu, J. Y. Wang, Y. Zhang, Y. L. Wan, D. P. Cao, D. O'Hare and Q. Wang, *Sci. Bull.*, 2017, **62**, 686–692.
141 Y. P. Zhang, H. P. Li, N. Du, S. E Song and W. G. Hou, *Appl. Clay Sci.*, 2017, **143**, 336–344.

142 Y. P. Zhang, X. W. Wu, H. P. Li, N. Du, S. E. Song and W. G. Hou, *Colloids Surf., A*, 2017, **529**, 824–831.
143 S. Q. Liu, S. P. Li and X. D. Li, *Appl. Surf. Sci.*, 2015, **330**, 253–261.
144 Z. L. Liu, Q. Y. Jia, X. F. Zhao, S. P. Li, J. Shen and X. D. Li, *Chem. Res. Chin. Univ.*, 2019, **35**(5), 901–907.
145 X. Mei, T. T. Hu, Y. J. Wang, X. S. Weng, R. Z. Liang and M. Wei, *Wiley Interdiscip. Rev.: Nanomed. Nanobiotechnol.*, 2019, **12**, e1596.
146 J. Y. Wang, W. L. Bao, A. Umar, Q. Wang, D. O'Hare and Y. L. Wan, *J. Biomed. Nanotechnol.*, 2016, **12**, 922–933.
147 X. W. Wu, H. P. Li, S. E. Song, R. J. Zhang and W. G. Hou, *Int. J. Pharm.*, 2013, **454**, 453–461.
148 X. Mei, S. M. Xu, T. Y. Hu, L. Q. Peng, R. Gao, R. Z. Liang, M. Wei, D. G. Evans and X. Duan, *Nano Res.*, 2018, **11**, 195–205.
149 L. Q. Peng, X. Mei, J. He, J. K. Xu, W. K. Zhang, R. Z. Liang, M. Wei, D. G. Evans and X. Duan, *Adv. Mater.*, 2018, 1707389.
150 L. Yan, M. J. Zhou, X. J. Zhang, L. B. Huang, W. Chen, V. A. L. Roy, W. J. Zhang and X. F. Chen, *ACS Appl. Mater. Interfaces*, 2017, **9**(39), 34185–34193.